

## Dynamics of homogeneous bubbly flows Part 2. Velocity fluctuations

By BERNARD BUNNER<sup>1</sup> AND GRÉTAR TRYGGVASON<sup>2</sup>

<sup>1</sup>Coventor, Inc., Cambridge, MA 02138, USA

<sup>2</sup>Mechanical Engineering Department, Worcester Polytechnic Institute, Worcester,  
MA 01609-2280, USA

(Received 14 March 2000 and in revised form 5 March 2002)

Direct numerical simulations of the motion of up to 216 three-dimensional buoyant bubbles in periodic domains are presented. The bubbles are nearly spherical and have a rise Reynolds number of about 20. The void fraction ranges from 2% to 24%. Part 1 analysed the rise velocity and the microstructure of the bubbles. This paper examines the fluctuation velocities and the dispersion of the bubbles and the ‘pseudo-turbulence’ of the liquid phase induced by the motion of the bubbles. It is found that the turbulent kinetic energy increases with void fraction and scales with the void fraction multiplied by the square of the average rise velocity of the bubbles. The vertical Reynolds stress is greater than the horizontal Reynolds stress, but the anisotropy decreases when the void fraction increases. The kinetic energy spectrum follows a power law with a slope of approximately  $-3.6$  at high wavenumbers.

---

### 1. Introduction

We report the results of direct numerical simulations of systems of buoyant bubbles containing up to 216 bubbles in triply periodic domains. The governing parameters were selected to give nearly spherical bubbles that rise with a Reynolds number of 12–30, depending on the void fraction, which ranges between 2% and 24%. In Bunner & Tryggvason (2002*a*), henceforth referred to as Part 1, the motion of the bubbles and the microstructure were analysed. It was found that the rise velocity decreases as the void fraction increases and that bubble pairs tend to align themselves horizontally.

Here, in Part 2, the fluctuation velocities and the dispersion of the bubbles are examined in §3.1 and §3.2, respectively. The unsteady motion of bubbles through an otherwise quiescent liquid results in an unsteady velocity field due to the displacement of the liquid by the bubble motion. This unsteady flow is often referred to as ‘pseudo-turbulence’ to distinguish it from ‘real’ turbulence, such as grid turbulence, caused by unsteady vortical flow at high Reynolds number. In engineering modelling of dispersed multiphase flows, averaging of the equations of motion results in the appearance of Reynolds stress terms even for low-Reynolds-number flows. While high-Reynolds-number, turbulent bubbly flows in pipes have been studied extensively, only a few papers deal with homogeneous turbulent flows (Serizawa, Kataoka & Michiyoshi 1975; Lance & Bataille 1991; van Wijngaarden 1998). In particular, Lance & Bataille (1991) have shown that the contributions of the turbulence in the liquid and the pseudo-turbulence due to the bubbles are only additive at void fractions below a value of about 1%. For higher void fractions, the turbulence is strongly amplified due to the hydrodynamic interactions between the bubbles. The complexity of bubbly

flows therefore warrants the study of laminar bubbly flows, for which no work is available in the literature, to the knowledge of the authors. This is discussed in §3.3. One particularly important issue, addressed in §3.4, is the existence of a universal kinetic energy spectrum, on which current turbulence models of bubbly flows, which are usually extensions of the  $k - \epsilon$  model, rely.

## 2. Problem formulation

We consider the three-dimensional motion of a triply periodic monodisperse array of buoyant bubbles with equivalent diameter  $d$ , radius  $a$ , density  $\rho_b$ , viscosity  $\mu_b$  and uniform surface tension  $\sigma$  in a fluid with density  $\rho_f$  and viscosity  $\mu_f$ . The array of bubbles is repeated periodically in the three spatial directions with periods equal to  $L$ . In addition to the acceleration due to gravity,  $\mathbf{g}$ , a uniform acceleration is imposed on the fluid inside and outside the bubbles to compensate for the hydrostatic head, so that the net momentum flux through the boundaries of the computational domain is zero.

The non-dimensional parameters describing the flow are the Eötvös number (sometimes also called Bond number),  $Eo = \rho_f g d^2 / \sigma$ , the Galileo or Archimedes number,  $N = \rho^2 g d^3 / \mu^2 = Eo^{3/2} / Mo^{1/2}$ , the void fraction  $\alpha$ , and the ratios of the densities and viscosities of the fluid in the bubble and in the continuous phase,  $\rho_b / \rho_f$  and  $\mu_b / \mu_f$ . For given fluids, the Eötvös number is a characteristic of the bubble size. The Galileo number is a Reynolds number squared based on the velocity scale  $(gd)^{1/2}$ . The Morton number,  $M = g \mu_f^4 / \rho_f \sigma^3$ , is sometimes used instead of the Galileo number. In this paper, we selected  $Eo = 1$  and  $N = 900$ , which results in a rise Reynolds number of about 36.0 in an unbounded flow. For computational reasons, the density and viscosity ratios are taken to be 1/50. It is shown in §2.7 of Part 1 that these finite ratios have insignificant effects on the results and that the results are representative of typical gas–liquid flows where the density and viscosity ratios may be lower.

Both regular arrays, where the periodic cell contains only one bubble, and free arrays, where two or more bubbles are included in the periodic cell, are considered. For free arrays, the number of bubbles in the cell,  $N_b$ , is an additional parameter of the problem. Results are presented for values of  $N_b$  ranging from 4 to 216. It was found in Part 1 that a good estimate of the average rise velocity can be achieved with as few as 12 bubbles.

In typical bubbly flows, surfactants affect the behaviour of the bubbles. We assume that surfactants are absent so that the interface is shear stress free. Since we are interested in steady-state average quantities, we also assume that the number of bubbles is constant by preventing the bubbles from coalescing (Part 1, §2.2). Both coalescence and the presence of surfactants can be included in the numerical method, but they represent added complexities and it is important to first develop a thorough understanding of flows where they are not present.

The numerical method is a front tracking/finite difference method originally developed by Unverdi & Tryggvason (1992) and described in more detail in §2.2 of Part 1 and Tryggvason *et al.* (2001). A single incompressible Navier–Stokes equation is solved over the entire flow domain. The interface between the fluids inside the bubble and the outer fluid is tracked explicitly by a moving mesh, or front, and the density and viscosity fields are reconstructed at each time step from the position of the front. The surface tension is added as a smoothed delta function onto the grid and it can be verified that the usual statements of continuity are satisfied at the interface. A number of validation tests are reported in the references. The definitions

of the bubble velocity  $V_b$ , slip or relative velocity  $V_r$ , drift velocity  $V_d$ , fluctuation velocity  $V'_b$  and the liquid Reynolds stress  $\langle u'_i u'_j \rangle$  are given in §2.3 of Part 1. The vertical relative velocity  $W_r$  will be used to scale the fluctuation velocities. From the condition that the mass-averaged velocity of the mixture is zero (Part 1, §2.2),  $V_m = (\alpha\rho_b V_b + (1 - \alpha)\rho_f V_f)/(\alpha\rho_b + (1 - \alpha)\rho_f) = 0$ , and the ratio of the densities,  $\rho_b/\rho_f = 1/50$ , it is easy to verify that  $W_r$  and  $W_b$  differ by less than 0.6% in all cases considered here. Note that the drift velocity  $W_d$  is used to report the mean rise velocity of the bubbles and that it is related to the relative velocity by  $W_d = (1 - \alpha)W_r$ . Grid-independence studies (Part 1, §2.4) showed that the resolutions employed for the simulations lead to errors in the Reynolds stresses of about 5% for  $\alpha = 24\%$  and 2% for  $\alpha \leq 12\%$ . Because of its prohibitive cost, no grid-independence study was performed in three dimensions with many bubbles to determine resolution requirements for the fluctuation velocities of the bubbles, but a less computationally expensive two-dimensional grid-independence study was performed and indicated that the errors in the fluctuation velocities are smaller than the errors in the Reynolds stresses (although we note that statistical variability due to finite averaging times and small system sizes may lead to significant errors, as discussed later).

The initial configuration of the  $N_b$  bubbles in the free arrays is a perturbed regular array, as explained in Part 1, §3. The simulations are conducted over sufficiently long periods of time that well-defined statistical results are obtained and that the steady-state results do not depend on the initial conditions.

### 3. Results

A table containing a list of the simulations of the free arrays, along with the computational requirements and timings of the simulations, is given in Part 1, §3.

#### 3.1. Bubble velocity fluctuations

Many bubbles rising together due to buoyancy do not move with a constant velocity but instead experience diffusion-like fluctuations in velocity due to interactions with neighbouring bubbles. In the potential flow simulations of Sangani & Didwania (1993), Smereka (1993), and Yurkovetsky & Brady (1996), the bubble velocities become equal when viscous dissipation is included. This is not observed in experiments or in our direct numerical simulations. The average velocity fluctuations in the vertical direction,  $W'_b$ , and in the horizontal direction,  $(U_b'^2 + V_b'^2)^{1/2}$ , are plotted versus time in figure 1 for the different values of  $N_b$  at  $\alpha = 6\%$  and in figure 2 for the different values of  $\alpha$  and  $N_b = 27$ . The variations of the fluctuation velocities are much larger than those of the rise velocities, with both long- and short-wave components. A Fourier transform of the fluctuation velocities of the individual bubbles reveals a continuously varying spectrum. In particular, no peak corresponding to a mean encounter time between bubbles can be determined. However, high-frequency components of the spectrum increase with the void fraction, which is consistent with the increased frequency of interaction between the bubbles. In the initial rise transient,  $W'_b$  remains very small until the perturbed array breaks up and then typically increases sharply while the bubbles rearrange themselves before settling down to a statistical steady state. The fluctuation velocities exhibit a strong dependence on both system size and void fraction.

For solid particles sedimenting in Stokes flow, Caflish & Luke (1985) initiated a still unresolved controversy by showing that the variances of the fluid and particle velocities increase like  $N_p^{1/3}$  as the number of particle  $N_p$  increases. Among the assumptions

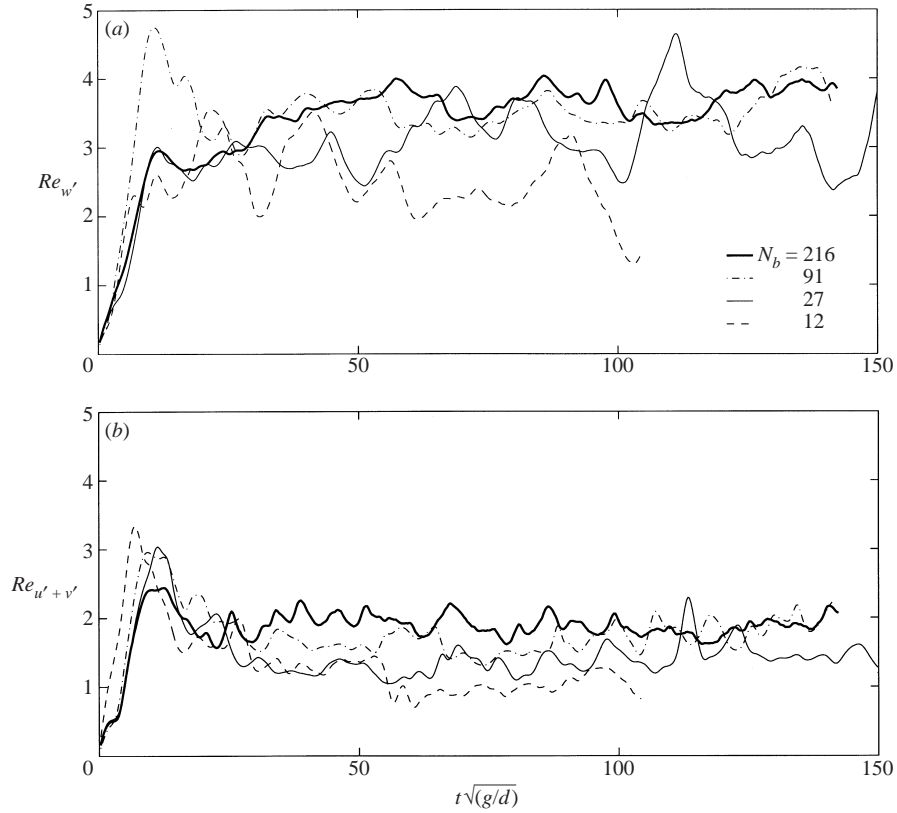


FIGURE 1. Average fluctuation velocities in the (a) vertical and (b) horizontal directions vs. time for different values of  $N_b$  at  $\alpha = 6\%$ . Notation:  $Re_{w'} = \rho_f W_b' d / \mu_f$  and  $Re_{u'+v'} = \rho_f (U_b'^2 + V_b'^2)^{1/2} d / \mu_f$ , where  $(U_b', V_b', W_b')$  are the fluctuating components of the bubble velocities, defined in Part 1, §2.3.

leading to this result are the neglect of inertia, absence of walls, consideration of two-particle interactions only, and a random particle distribution. Various screening mechanisms were devised in order to render the variance finite. Koch & Shaqfeh (1991) suggested that screening results from correlations in the particle distribution. They found that a distribution characterized by a net deficit of one particle in the neighbourhood of a test particle can lead to finite velocity fluctuations. Numerical simulations with up to 108 particles using a multipole method (Ladd 1993) and with up to 32 768 particles using a lattice-Boltzmann approach (Ladd 1997) did not show the deficit predicted by the Koch–Shaqfeh (1991) theory, nor did they show convergence of the velocity fluctuations when the system size increases. Convergence was observed in the experiments of Ham & Homsy (1988), Nicolai & Guazzelli (1995), Nicolai *et al.* (1995), and Segré, Herbolzheimer & Chaikin (1997). Brenner (1999) explored the effect of walls on the velocity fluctuations and concluded that this effect does not exclude the possibility of divergence when the system size increases. He also proposed another screening mechanism based on a cutoff of the slow decay in  $r^{-1}$  of the velocity induced by a particle. His argument is that, when the velocity fluctuations reach a certain level, particle diffusion becomes larger than the momentum diffusion due to viscosity. At this point, momentum transport through diffusion away from the particles is no longer effective, and  $\mathbf{u} \sim r^{-1}$  is not valid anymore.

For bubbles and particles at  $Re \sim O(1)$ , where the Oseen approximation can be

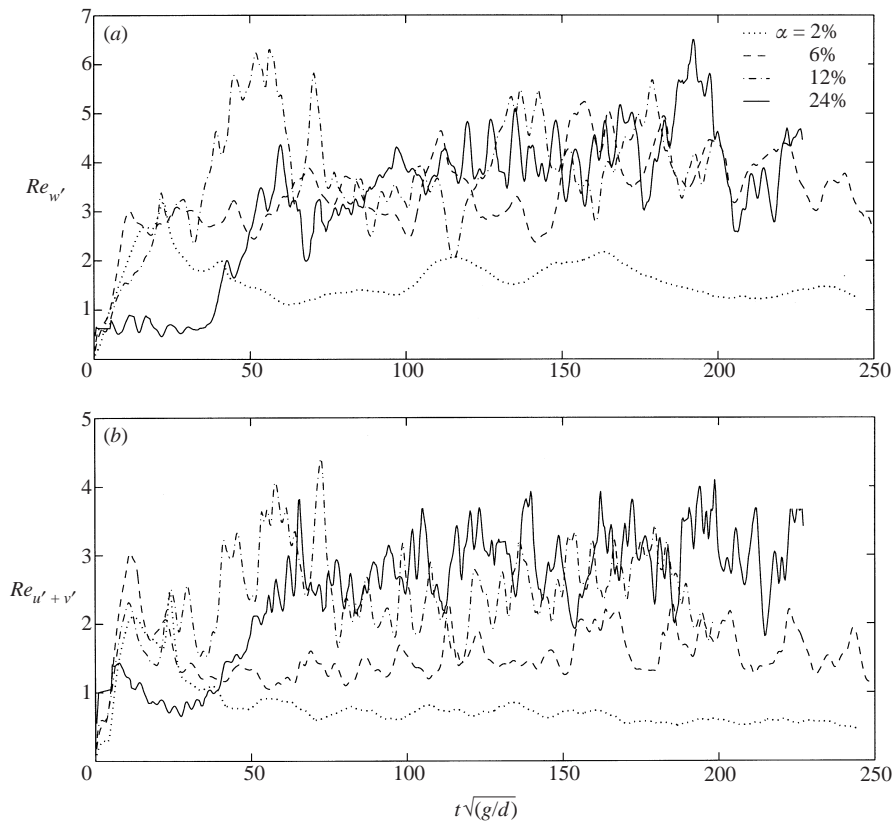


FIGURE 2. Average fluctuation velocities in the (a) vertical and (b) horizontal directions vs. time for different values of  $\alpha$  at  $N_b = 27$ . The notation is the same as in figure 1.

used, Koch (1993) showed that the velocity fluctuations are screened by buoyancy screening, as described below. In the Oseen solution, the velocity decays like  $r^{-2}$  outside the wake but  $r^{-1}$  in the wake, which causes a logarithmic divergence in the velocity fluctuations. Koch (1993) argued that the lift force tends to retard advection of particles into the wake of a test particle, which leads to a deficit of particles in the centre of the wake of the test particle and to screening of the velocity fluctuations at a finite distance behind the particle. Such a deficit was indeed observed in experiments by Cartellier & Rivière for  $Re \sim O(10)$  (but not for  $Re \sim O(1)$ ), together with a slight accumulation of bubbles on the border of the wake.

When the potential flow model is used to determine the motion of bubbles in the limit of high Reynolds number and low Weber number, the velocity disturbance created by a bubble decays like  $r^{-3}$ , so that the variance is expected to converge as  $N_b$  increases. The question of how large the system must be in order to provide results that are independent of  $N_b$  has, to our knowledge, not been addressed in the literature. However, simulations of the motion of spherical bubbles in potential flow in the absence of gravity and viscosity (Smereka 1993) showed a small but noticeable increase in the mean value of the variance between  $N_b = 50$  and 200, as well as large fluctuations in time (when gravity and viscosity are included, the variance decays towards zero, as noted previously). These findings are consistent with our results. Both the horizontal and the vertical velocity fluctuations in figure 3

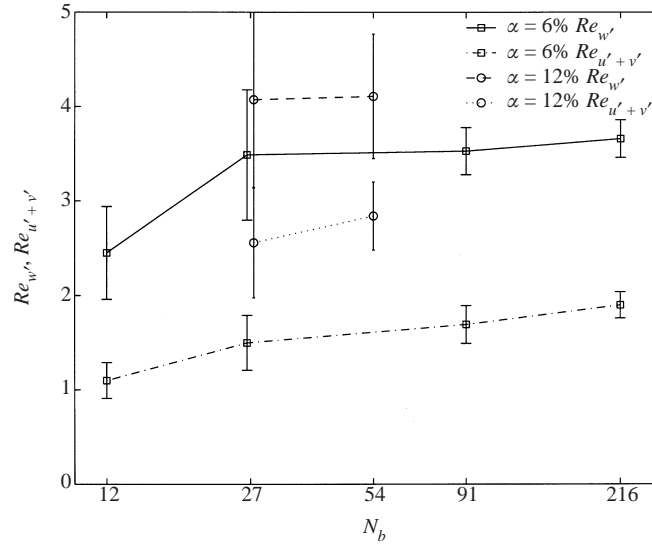


FIGURE 3. Effect of system size on the mean velocity fluctuations at  $\alpha = 6\%$  and  $12\%$ . The notation is as in figure 1. The average values are determined over the time intervals  $[T_i, T_f]$  defined in table 4 of Part 1. The error bars represent the standard deviation of the data over this time interval.

increase when the system becomes larger. Although it is not possible to determine the large- $N_b$  limits, we note that the rates of increase become smaller as  $N_b$  increases. Furthermore, the results of Part 1, § 3.3 indicate a deficit of bubbles in the wake of each bubble. Therefore, according to Koch's (1993) theory, the fluctuations velocities should converge.

The mean velocity fluctuations are also strong functions of the void fraction, as shown in figure 4.  $W_b'$  increases until  $\alpha = 12\%$  and remains approximately constant for  $\alpha \geq 12\%$  (figure 4(a)). In contrast,  $(U_b'^2 + V_b'^2)^{1/2}$  increases in the entire  $[2\%, 24\%]$  interval; at  $24\%$ , it is equal to  $72\%$  of  $W_b'$ . This shows that energy is being transferred by the fluctuating motion of the bubbles from the vertical to the horizontal directions, a phenomenon which is also seen in the turbulence characteristics of the liquid phase. A similar trend in the variation of the anisotropy with void fraction is observed in experiments of settling solid particles in Stokes flow conditions (Nicolai *et al.* 1995). However, the velocity fluctuations relative to the mean velocity are much higher for sedimenting particles, where they reach up to  $170\%$  (Nicolai *et al.* 1995), than they are for the bubbles in our simulations, where  $W_b'/W_r$  is at most  $27\%$ . Increased isotropy of the bubble velocity fluctuations is also seen in studies of turbulent dispersion of bubbles when the turbulence intensity of the flow field increases (Spelt & Biesheuvel 1997, 1998). The only turbulence present in our simulations is the pseudo-turbulence generated by the motion of the bubbles.

Sangani, Zhang & Prosperetti (1991) considered the problem of a bubbly mixture subjected to a small-amplitude oscillatory motion. They determined the variance normalized by the mean amplitude of the bubble velocities in a dilute random array to leading order in  $\alpha$ ,

$$var = 0.275\alpha, \quad (3.1)$$

and obtained values at higher void fractions by dynamic simulations using a multipole method. They found that the variance reaches a maximum of approximately  $0.025$  at  $\alpha \approx 30\%$ . This is consistent with our results, where the variance increases in the

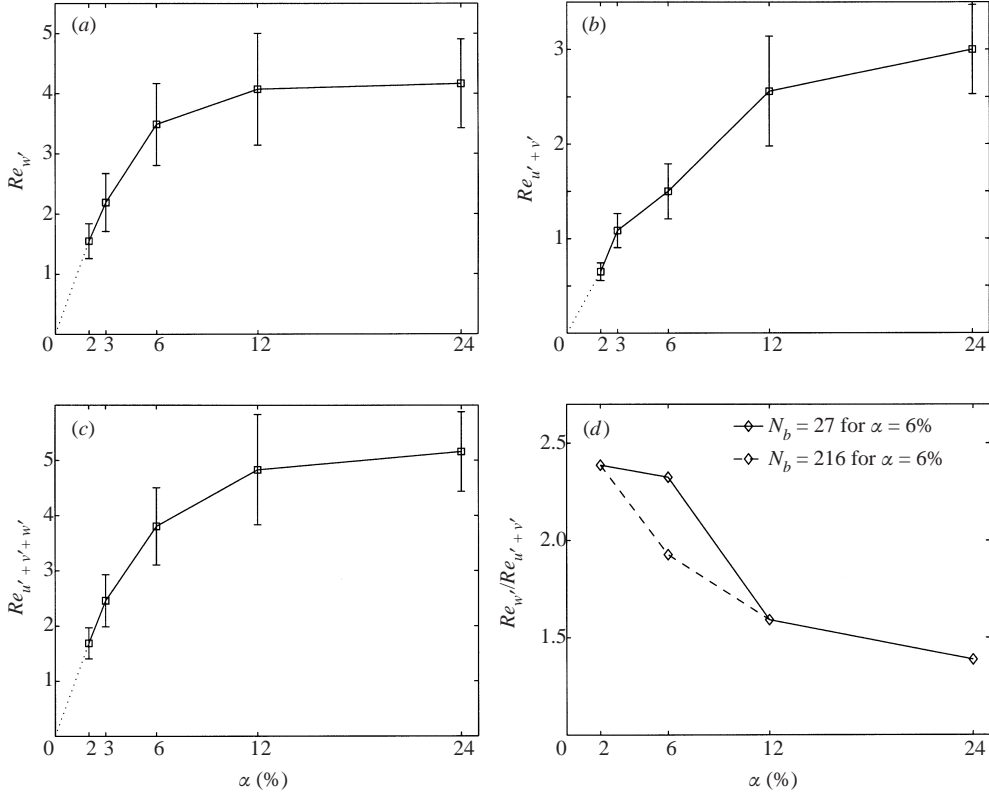


FIGURE 4. Effect of void fraction on the (a) vertical velocity fluctuations, (b) horizontal velocity fluctuations, and (c) total velocity fluctuations for  $N_b = 27$  ( $\alpha = 2\%$ ,  $6\%$ ,  $12\%$  and  $24\%$ ) and  $N_b = 13$  ( $\alpha = 3\%$ ). (d) Ratio of the vertical to the horizontal velocity fluctuations. The total velocity fluctuations are defined as  $Re_{u'+v'+w'} = \rho_f(U_b'^2 + V_b'^2 + W_b'^2)^{1/2}d/\mu_f$ .

entire  $[0, 24\%]$  interval. The variance is, however, significantly higher in our results, where it is equal to 0.11 at  $\alpha = 24\%$ .

In figure 5(a), the variance scaled by the square of the slip velocity is shown versus  $\alpha$ . We see that the variance is approximately a linear function of  $\alpha W_r^2$ , as was also observed in the experiments of Zenit, Koch & Sangani (2001). A linear fit,

$$Re_{u'+v'+w'}^2 = 0.54\alpha Re_r^2 - 0.0069, \quad (3.2)$$

where  $Re_{u'+v'+w'} = \rho_f(U_b'^2 + V_b'^2 + W_b'^2)^{1/2}d/\mu_f$ , is shown in figure 5(b). It appears that the variance depends in a nonlinear fashion on the void fraction between  $\alpha = 0$  and  $2\%$ , even when the spread in the data due to statistical variations is accounted for. In contrast, the velocity fluctuations in the liquid phase, i.e. the turbulent kinetic energy, is a linear function of the void fraction, as seen in § 3.3. The ratio of the vertical over horizontal velocity fluctuations, in figure 4(d), decreases with  $\alpha$ , although variations due to large statistical errors can be seen. In contrast, for solid particles (Nicolai *et al.* 1995), this ratio increases up to  $12\%$  and decreases for larger concentrations, although the values of the ratio are of the same order of magnitude.

Finally, it is interesting to relate the bubble velocity fluctuations to the microstructure. Spelt & Sangani (1998) determined the pair probability density for two bubbles in contact as a function of the angle between the line joining two bubbles

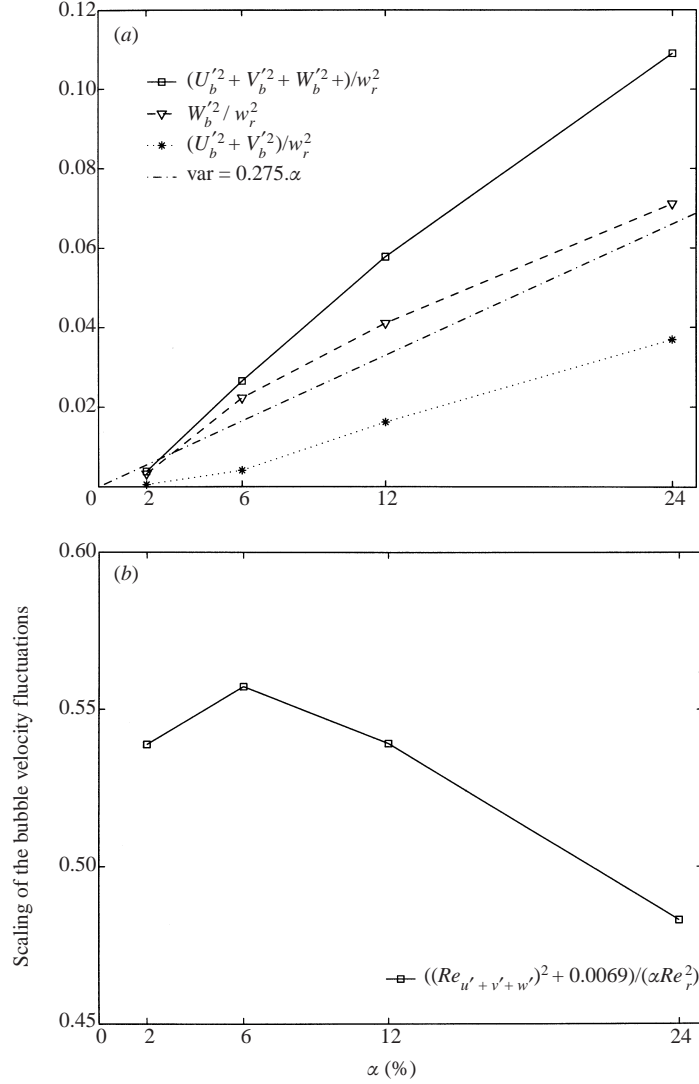


FIGURE 5. (a) Average bubble velocity fluctuations divided by the average relative velocity, plus the first-order expression in  $\alpha$  of Sangani *et al.* (1991). (b) Proposed scaling of the total velocity fluctuations:  $Re_{u'+v'+w'}^2 = 0.54\alpha Re_r^2 - 0.0069$ , where  $Re_{u'+v'+w'}$  is defined in figure 4.

and the vertical direction (i.e.  $G(\theta)$  at  $r = 2a$ , using the notation defined in Part 1, § 3.3) by potential flow simulations, where the mean rise velocity and the mean bubble velocity variance are imposed. Similarly to our results, they found a peak in  $G(\theta)$  at  $\theta = \pi/2$ , indicative of a preference for an horizontal alignment of bubble pairs. They also found that the peak value decreases when the fluctuation velocities increase. Both of these findings are consistent with our results. However, there are also significant differences. The velocity fluctuations are nearly isotropic in Spelt & Sangani (1998), whereas they are strongly anisotropic in our results. Also, the bubbles do not touch each other when the void fraction is low in our simulations, whereas the very definition of the pair probability adopted by Spelt & Sangani (1998) assumes that they do, for dilute as well as for dense flows.



## 3.2. Hydrodynamic dispersion of the bubbles

The dispersion of the bubbles is characterized by the mean value of the bubble velocity fluctuations and the relaxation time of their autocorrelation function. The theory of the dispersion of fluid points in a homogeneous stationary turbulent flow was laid out by Taylor (1921). Taylor showed that the mean-square displacement of a marked fluid particle is given by

$$\overline{X(T)^2} = 2\overline{u^2} \int_{T_0}^T dt \int_0^t R(\tau)_u d\tau, \quad (3.3)$$

where  $R(\tau)_u = \overline{u(t)u(t+\tau)}/\overline{u^2}$  is the Lagrangian autocorrelation function of the fluctuating velocity  $u(t)$  following a fluid point. He also showed that  $\overline{X(T)^2} = 2\overline{u^2}T_L(T - T_0)$  for  $(T - T_0) \gg T_L$ , where  $T_L = \int_0^\infty R(\tau)_u d\tau$  is the Lagrangian integral time scale. Batchelor & Townsend (1956) recognized that, as for random-walk problems, a linear variation of the dispersion  $\overline{X(T)^2}$  with time is associated with a Gaussian probability distribution  $Q(X)$  of the displacements  $X$ . This is equivalent to the statement that  $Q$  satisfies a diffusion equation

$$\frac{\partial Q}{\partial t} = D \frac{\partial^2 Q}{\partial X^2}, \quad (3.4)$$

where the diffusion coefficient or dispersion coefficient  $D$  is given by

$$D = \overline{u^2} T_L = \lim_{T \rightarrow \infty} \frac{1}{2} \frac{d\overline{X^2(T)}}{dT}. \quad (3.5)$$

$D$  can also be determined using the pseudo-coefficient

$$D = \lim_{T \rightarrow \infty} \frac{\overline{X^2(T)}}{2(T - T_0)}. \quad (3.6)$$

These equations are applicable for the dispersion of particles or bubbles if  $u$  is the fluctuating component of the velocity of the particles or bubbles instead of the fluctuating velocity of a fluid point and if the displacements have a Gaussian probability distribution. The Lagrangian integral scale  $T_L$  is a measure of the time of statistical persistence of the velocity of the particle and the length  $\overline{u^2}^{1/2} T_L$  is a measure of the distance travelled by the particle during this time. The dispersion of particles and bubbles is generally anisotropic and therefore described by a dispersion tensor. This dispersion tensor is used in two-fluid models of multiphase flows to express the continuity equation of the dispersed phase as

$$\frac{\partial(\epsilon\rho)}{\partial t} + \nabla \cdot (\epsilon\rho\mathbf{u}) = \nabla \cdot D\nabla(\epsilon\rho) \quad (3.7)$$

(Crowe, Troutt & Chung 1996; Sokolichin *et al.* 1999), where  $\epsilon$ ,  $\rho$  and  $\mathbf{u}$  are respectively the local void fraction, the density and the velocity of the dispersed phase. However, for this simple dispersion model to be valid, it is necessary to prove that the statistics of the bubble motion are Gaussian.

Due to the difficulty of measuring Lagrangian statistical properties in experiments, the only available data in the literature for the dispersion of bubbles are the studies of turbulent transport of Serizawa *et al.* (1975), Spelt & Biesheuvel (1997, 1998) and Poorte (1998). Although direct comparisons with results for solid particles are not possible, it is nevertheless instructive to look at our results in view of the literature for particles, which is richer than the one for bubbles. Since we are interested

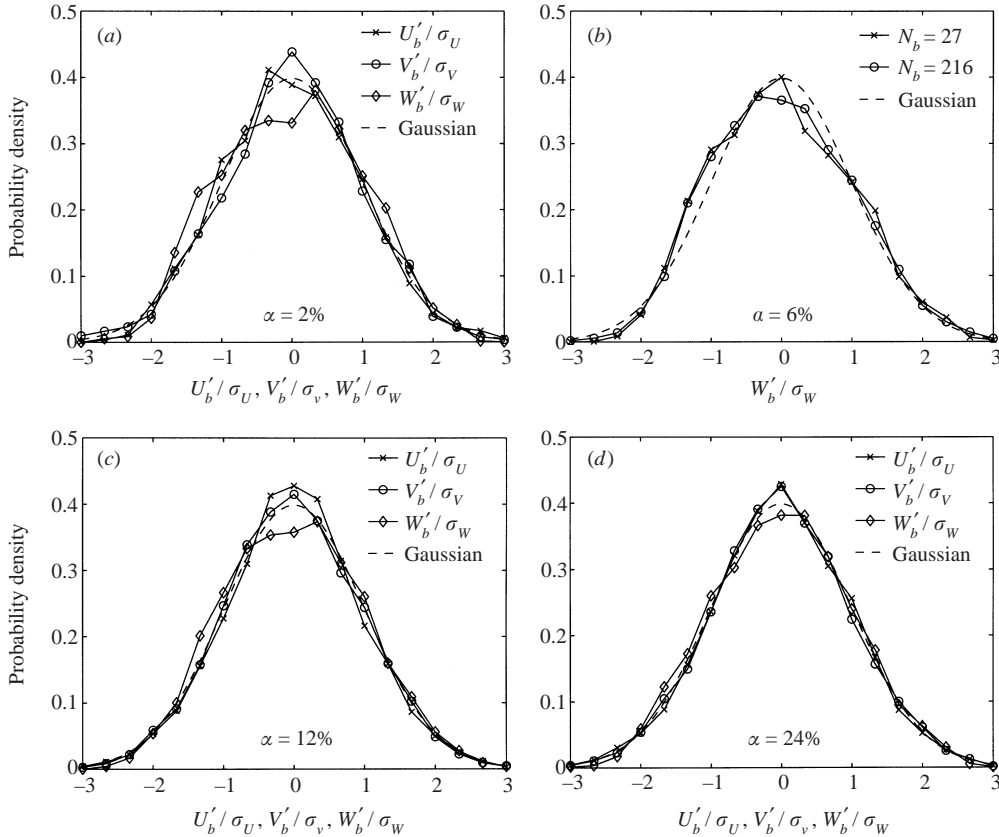


FIGURE 6. Probability density functions of the bubble velocity fluctuations for (a)  $\alpha = 2\%$ ,  $N_b = 27$ , (b)  $\alpha = 6\%$ ,  $N_b = 27$  and 216, (c)  $\alpha = 12\%$ ,  $N_b = 27$ , and (d)  $\alpha = 24\%$ ,  $N_b = 27$ . In (b), only the p.d.f. of  $W'_b$  is shown; the p.d.f.s of  $U'_b$  and  $W'_b$  are similar to those at  $\alpha = 12\%$  and  $24\%$ . The velocity fluctuations are scaled by their standard deviations,  $\sigma_U$ ,  $\sigma_V$ , and  $\sigma_W$ , and  $[-3\sigma, +3\sigma]$  is discretized into 19 intervals.

in self-diffusion in a homogeneous flow, we only mention the related studies of diffusion induced by a gradient of concentration (Davis & Hassen 1988; Nitsche & Batchelor 1997), by shear (Eckstein, Bailey & Shapiro 1977; Leighton & Acrivos 1987; and Acrivos *et al.* 1992), and by turbulence (Snyder & Lumley 1971; Squires & Eaton 1990; Elghobashi & Truesdell 1992; Wang & Maxey 1993). A review of the hydrodynamic dispersion of suspended particles is given by Davis (1996). Relevant studies of the self-dispersion of particles include Ham & Homsy (1988), Ladd (1993, 1997), Nicolai *et al.* (1995), and Parthasarathy & Faeth (1990a,b).

The probability density functions (p.d.f.) of  $U'_b$ ,  $V'_b$  and  $W'_b$  are shown in figure 6 for the different values of  $\alpha$  and  $N_b$ . Since the displacements of the bubbles are time integrals of their velocities, the p.d.f. of the displacements is Gaussian if the p.d.f. of the velocities is Gaussian. The velocities are normalized by their respective standard deviations,  $\sigma_U$ ,  $\sigma_V$  and  $\sigma_W$ , and the  $N(0, 1)$  Gaussian p.d.f. is superposed on the plots for reference. We checked that the results are insensitive to the number of time samples and the number of intervals on the horizontal axis. However, it is likely that the results are somewhat affected by the limited system size and simulation time.

Even though small differences can be seen in figure 6 for the different values of  $N_b$  and  $\alpha$ , in particular in the interval  $-\sigma_W < W'_b < \sigma_W$ , the qualitative trends are

the same. The curves of the p.d.f. of  $W'_b$  are slightly asymmetric and lie above the  $N(0, 1)$  curve for  $-2\sigma_W < W'_b < -0.5\sigma_W$ , but below it for  $-0.5\sigma_W < W'_b < 0.5\sigma_W$ . This can be explained by the preponderance of horizontally aligned bubble pairs, whose rise velocity is less than the average rise velocity, as seen in figure 16 of Part 1. For  $W'_b < -2\sigma_W$ , the p.d.f. of  $W'_b$  lies below the Gaussian p.d.f., indicating a scarcity of bubbles with a very low rise velocity. This is also consistent with the observations made in §3.3 of Part 1 concerning figure 16. In contrast, the p.d.f.s of  $U'_b$  and  $V'_b$  are roughly symmetric, although their shape is slightly narrower than the shape of the Gaussian p.d.f. and their peak lies above that of  $N(0, 1)$ . Spelt & Biesheuvel (1997, 1998) determined the p.d.f. of the bubble velocities by kinematic simulation for very dilute bubbly flows in an imposed turbulent flow field and Poorte (1998) performed the corresponding experiments. The results of Spelt & Biesheuvel (1997, 1998) and Poorte (1998) agree well with each other, but show significant differences from our results. They report that the p.d.f. of  $W'_b$  is also asymmetric, but with a maximum at  $W'_b > 0$  instead of  $W'_b < 0$ , and that the values of the p.d.f. for  $W'_b \ll 0$  are greater than those of the Gaussian p.d.f. Poorte (1998) attributes the large probability at  $W'_b \ll 0$  to the preferential attraction of bubbles to downflow regions due to the lift force. The difference between the results of Spelt & Biesheuvel (1997, 1998) and Poorte (1998) and our results can be attributed to the very different flow conditions. The void fractions in our simulations are much larger than in their experiments and simulations and the Reynolds number is much lower. In addition, the external forcing by a turbulent flow, which is responsible for the creation of large-scale flow structures such as downflow regions in their studies, is absent from our simulations, where dispersion is primarily due to the hydrodynamic interactions of the bubbles.

As the void fraction increases, the p.d.f. of  $W'_b$  generally becomes closer to the Gaussian curve, except in the interval  $-\sigma_W < W'_b < \sigma_W$ , where significant differences remain. The effect of system size, illustrated in figure 6(b) for  $N_b = 27$  and 216, is small, except again in the  $-\sigma_W < W'_b < \sigma_W$  interval. Assuming the dispersion process of the bubbles to be a Gaussian diffusion process is apparently a good first-order approximation. Ham & Homsy (1998), Parthasarathy & Faeth (1990b), Ladd (1993) and Nicolai *et al.* (1995) all mention that the p.d.f. of the particle velocity fluctuations are approximately Gaussian, although Ladd (1993) adds that there are significant non-Gaussian effects at high volume fractions, and Parthasarathy & Faeth (1990b) report flatness factors between 3.5 and 6.3. In comparison, the flatness factor for the results of figure 6 is between 2.3 and 3.5.

Another method to evaluate whether the dispersion process can be approximated as a diffusion process is to see if the pseudo-coefficient  $D'_i(T) = \overline{X_i^2(T)}/2(T - T_0)$  converges towards a constant value as  $T$  increases.  $D'_x(T) + D'_y(T)$  and  $D'_z(T)$  are shown in figure 7. They are determined by averaging over the  $[T_i, T_f]$  interval in order to avoid the initial transient:

$$D'_i(T) = \frac{1}{T_f - T_i - T} \int_{T_i}^{T_f - T} \overline{\frac{X_i^2(T | T_0)}{2(T - T_0)}} dT_0. \quad (3.8)$$

The mean values,  $D'_x + D'_y$  and  $D'_z$ , are determined over the  $[T_i + 0.5(T_f - T_i), T_i + 0.9(T_f - T_i)]$  interval and are shown in figure 7 by horizontal lines.

Although the limited simulation time and system size lead to a large uncertainty in their estimation, the dispersion coefficients seem to converge in time. Therefore the dispersion process can be characterized by a diffusion model. The same result was found by Serizawa *et al.* (1975) in experiments on turbulent transport of air bubbles

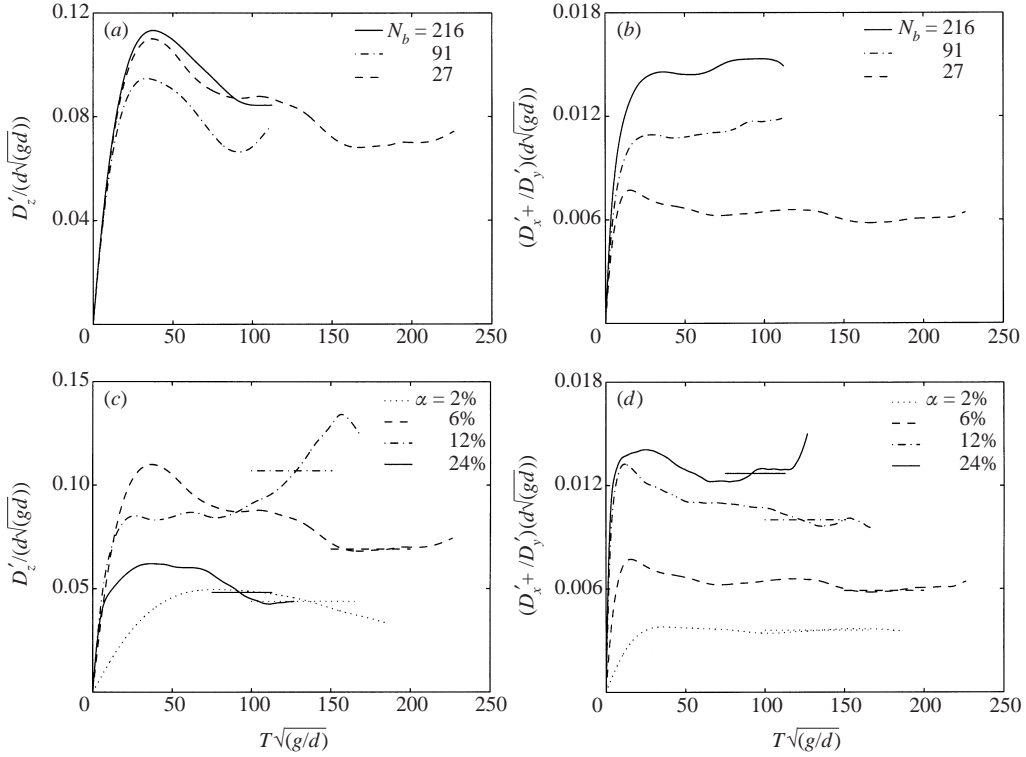


FIGURE 7. Dispersion coefficients versus time. (a) Vertical coefficient  $D'_z$  and (b) horizontal coefficient  $D'_x + D'_y$  for different system sizes at  $\alpha = 6\%$ . (c) Vertical coefficient  $D'_z$  and (d) horizontal coefficient  $D'_x + D'_y$  for different void fractions and  $N_b = 27$ ; the mean values are superposed along with the interval on which they are determined.

in water. The horizontal pseudo-coefficients converge faster in time than the vertical pseudo-coefficients, which is consistent with the results for the probability densities. Like the velocity fluctuations, system size effects are more pronounced for  $D'_x + D'_y$  than for  $D'_z$ .  $D'_x + D'_y$  increases by a factor of 2.5 between  $N_b = 27$  and  $N_b = 216$ . The individual values of  $D'_x$  and  $D'_y$ , not shown, which should be equal in view of the symmetry of the problem, differ by up to 20% for  $N_b = 27$ , but the difference is smaller when the system is larger. We also checked that the off-diagonal components of the dispersion tensor,  $D'_{xy}(T)$ ,  $D'_{xz}(T)$  and  $D'_{yz}(T)$ , which should be zero if  $N_b$  or the simulation time were infinitely large, are much smaller than the diagonal components.

The dependence of the dispersion coefficients on the void fraction is illustrated in figure 8(a,b), using only the results for  $N_b = 27$ , for consistency.  $D'_z$  increases until  $\alpha = 12\%$ , where it reaches a maximum of  $D'_z \approx 0.3aW_r$ . Although the self-diffusivities of solid particles reported in the experimental studies of Ham & Homay (1988) and Nicolai *et al.* (1995) and in the numerical simulations of Ladd (1993, 1997) are slightly different from each other, they are all larger than the values found for the bubbles in our simulations by a factor of at least twenty. Ham & Homay (1988) find that the vertical diffusion coefficient reaches a maximum of  $D'_z \approx 6aW_s$  at  $\alpha = 5\%$ , where  $W_s$  is the mean settling velocity. Nicolai *et al.* (1995) find that  $D'_z \approx 10aW_s$  and  $D'_x + D'_y \approx 2aW_s$  in the  $10\% < \alpha < 30\%$  interval. The simulation results of Ladd (1993) are of the same order of magnitude but exhibit a strong dependence on

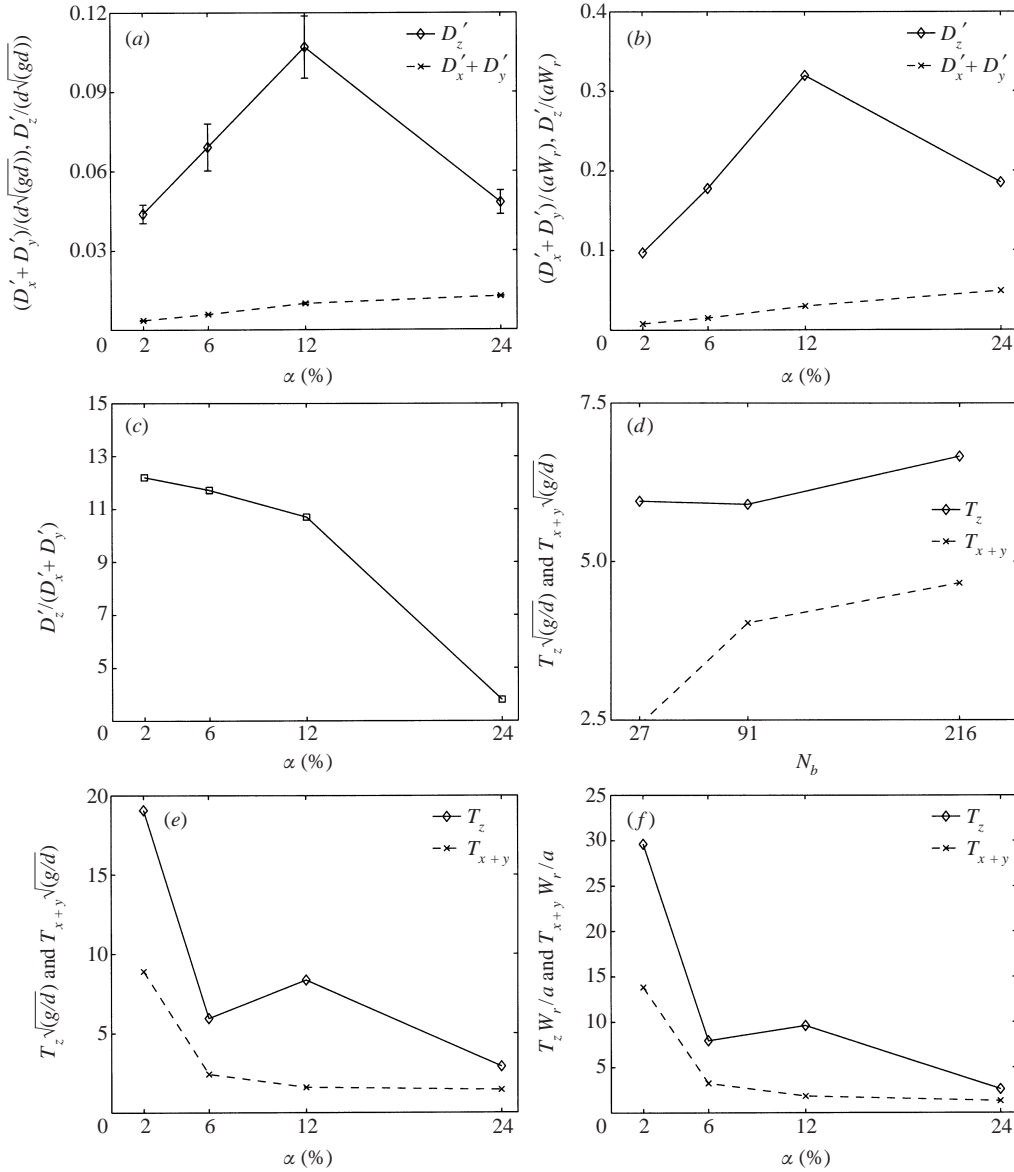


FIGURE 8. (a) Horizontal and vertical diffusion coefficients  $D'_z$  and  $D'_x + D'_y$  as a function of  $\alpha$ . (b) Same as (a), but normalized by the bubble radius and the mean bubble slip velocity. (c) Ratio of vertical to horizontal diffusion coefficients. (d) Vertical and horizontal Lagrangian integral time scales as a function of  $N_b$  for  $\alpha = 6\%$ . (e) Vertical and horizontal Lagrangian integral time scales  $T_z$  and  $T_{x+y}$  normalized by  $(gd)^{1/2}$  as a function of  $\alpha$ . (f) Same as (e), but the times are normalized by  $W_r/a$ . All the results, except those in (d), are for  $N_b = 27$ .

the number of particles  $N_p$ , since the normalized vertical dispersion coefficients are respectively 3.6 and 8 for  $N_p = 32$  and 108.

$D'_z$  is much larger than  $D'_x + D'_y$ . The ratio of  $D'_z$  over  $D'_x + D'_y$ , in figure 8(c), is greater than 10 for  $\alpha \leq 12\%$ . For  $\alpha = 24\%$ , this ratio is smaller, about 3.8, but still much larger than the ratio of the squares of the vertical and horizontal velocity fluctuations, which is about 1.9 at 24%. The anisotropy is greater than in the experiments of Nicolai

*et al.* (1995). The same observation is made in the numerical simulations of Ladd (1993), where the vertical coefficients are larger than the horizontal coefficients by two orders of magnitude. In both our study and in Ladd's (1993) study, it is possible that this very large anisotropy is due in part to system size effects, since it appears that the horizontal dispersion coefficients are more sensitive to  $N_b$  than the vertical dispersion coefficient.

Using the relations  $D'_z = \overline{W_b'^2} T_z$  and  $D'_x + D'_y = (\overline{U_b'^2} + \overline{V_b'^2}) T_{x+y}$ , the vertical and horizontal Lagrangian integral time scales  $T_z$  and  $T_{x+y}$  are determined and plotted in figure 8(d,e,f). The effect of system size is noticeable, but smaller than for the dispersion coefficients. The dependence of  $T_z$  and  $T_{x+y}$  on the void fraction is marked by an almost monotonic decrease in the [2%, 24%] interval, the values at 24% being smaller than the values at 2% by a factor of about 6. The integral time scales are anisotropic like the dispersion coefficients, but the ratio of the vertical and horizontal components is smaller and is approximately equal to 2.

The autocorrelation functions of the velocity fluctuations are determined according to

$$R(T)_{WW} = \frac{1}{T_f - T_i - T} \int_{T_i}^{T_f - T} \frac{W'_b(T_0)W'_b(T_0 + T)}{\overline{W_b'^2}} dT_0, \quad (3.9)$$

for  $T$  going from 0 to  $T_f - T_i$ . The autocorrelation functions of the horizontal and vertical velocities are shown in figure 9. The small number of sampling times as  $T$  approaches  $T_f - T_i$  and the limited size of the systems are the causes of the fluctuations seen in the plots, in particular when  $T$  becomes large. Therefore, while it should be possible to recover the values of the Lagrangian integral time scales determined above by integrating the autocorrelation functions, the large fluctuations of these autocorrelation functions when  $T$  is large prevents us from doing so. However, the Taylor microscales,  $\lambda_t$ , can be estimated with a reasonable degree of accuracy because they depend only on the behaviour of the autocorrelation functions close to  $T = 0$ , where a large number of time samples are available to determine the autocorrelation functions  $R(T)$ :

$$\lambda_t = -2 \left/ \frac{d^2 R(T)}{dT^2} \right|_{T_0}. \quad (3.10)$$

$\lambda_t$  is determined from a finite difference approximation of the derivative of  $R(T)$ . The Taylor microscales are shown in figure 10. Like the integral time scales, the Taylor microscales depend slightly on  $N_b$  and decrease with  $\alpha$ . The Taylor microscales are only slightly smaller than the integral time scales.

Comparisons of the autocorrelation functions for  $\alpha = 6\%$  and  $N_b = 27, 91$  and 216 reveal significant differences in the horizontal components at all values of  $T$ . Large differences are also observed for  $R(T)_{WW}$ , but they are mostly at large times, where statistical errors are large. Two general observations can be made about the results.

The first observation is that  $R(\tau)_{WW}$  becomes negative and seems to remain negative as it approaches zero. The same behaviour was seen in the molecular dynamics simulations of dense monoatomic liquids by Rahman (1964) and in the measurements of particle velocity autocorrelation functions in a turbulent flow by Snyder & Lumley (1971). Snyder & Lumley attribute this negative correlation to the 'correlation effect', i.e. the existence of a backflow necessary to satisfy continuity in the continuous phase. We note that Lagrangian dispersion models of solid particles usually follow the Langevin model of an exponentially decaying autocorrelation function (e.g. Sommerfeld, Kohnen & R ger *et al.* 1993). This exponential autocorrelation

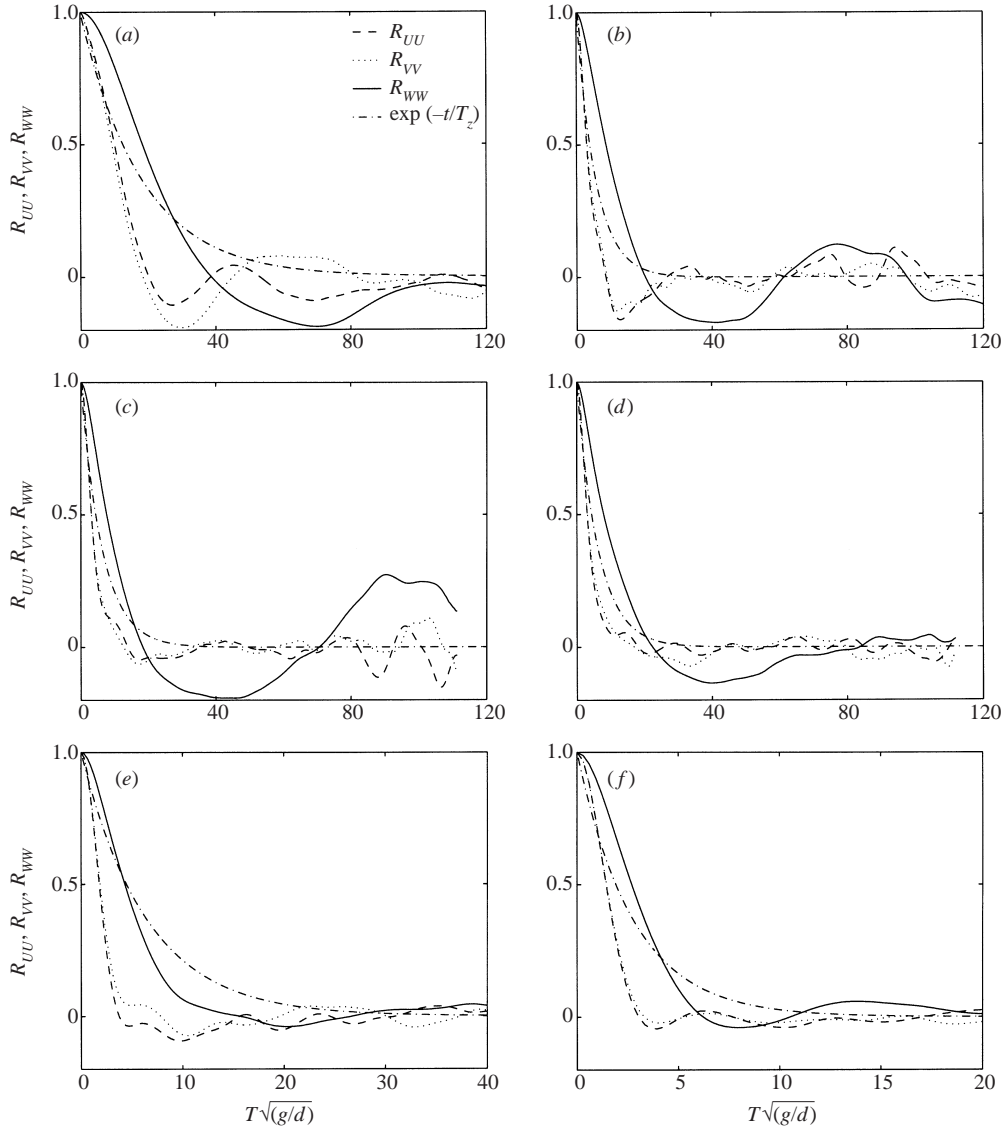


FIGURE 9. Autocorrelation functions  $R_{UU}$ ,  $R_{VV}$  and  $R_{WW}$  of the bubble velocity fluctuations versus  $T$ . (a)  $\alpha = 2\%$ ,  $N_b = 27$ ; (b)  $\alpha = 6\%$ ,  $N_b = 27$ ; (c)  $\alpha = 6\%$ ,  $N_b = 91$ ; (d)  $\alpha = 6\%$ ,  $N_b = 216$ ; (e)  $\alpha = 12\%$ ,  $N_b = 27$ ; (f)  $\alpha = 24\%$ ,  $N_b = 27$ .

function,  $\exp(-t/T_z)$ , is superposed in figure 9 for comparison, using the values of  $T_z$  determined above from the diffusion coefficients.

The second observation is that the vertical fluctuation velocities remain correlated for long periods of time. In the most dilute case,  $\alpha = 2\%$ ,  $R(\tau)_{WW}$  does not appear to have converged to zero by  $T = 120$ . When the motion of a particular bubble is tracked in the computer animation for  $\alpha = 2\%$ , we see that its path beyond the initial transient is nearly rectilinear and that strong interactions with neighbouring bubbles occur only two or three times in the  $[T_i, T_f]$  interval. This is consistent with the persistence in time of  $R(\tau)_{WW}$ . In general, the horizontal fluctuation velocities become uncorrelated earlier than the vertical fluctuations velocities and the correlation times

$\alpha$ (%)	$N_b$	$Re_d$	$Re_r$	$\frac{W'_b}{W_b}$	$\frac{(U'_b + V'_b)}{W_b}$	$\frac{D'_z}{aW_b}$	$\frac{(D'_x + D'_y)}{aW_b}$	$\frac{T_z W_b}{a}$	$\frac{T_{x+y} W_b}{a}$
2	27	26.60	27.14	0.0573	0.0240	0.0973	0.0080	29.6	13.8
3	13	25.10	25.88	0.0847	0.0420	—	—	—	—
6	2	25.85	27.50	—	—	—	—	—	—
6	4	20.19	21.48	—	—	—	—	—	—
6	12	21.86	22.98	0.1067	0.0479	—	—	—	—
6	27	21.95	23.35	0.1493	0.0683	0.1775	0.0152	7.95	3.25
6	91	22.19	23.61	0.1494	0.0717	0.1779	0.0280	7.98	5.44
6	216	22.39	23.82	0.1536	0.0797	0.2141	0.0403	9.07	6.35
12	27	17.68	20.09	0.2027	0.1273	0.3195	0.2990	9.61	1.84
12	54	17.93	20.38	0.2016	0.1394	—	—	—	—
24	27	11.87	15.62	0.2666	0.1921	0.1852	0.0488	2.60	1.30

TABLE 1. Transport properties of the bubbles. The values that are missing could not be determined either because the system was too small or the simulation time was too short.  $Re_d$  is the drift Reynolds number,  $Re_b$  the relative Reynolds number.  $U'_b$ ,  $V'_b$  and  $W'_b$  are the fluctuation velocities.  $D'_x + D'_y$  and  $D'_z$  are the horizontal and vertical diffusion coefficients, respectively.  $a$  is the bubble radius.  $T_{x+y}$  and  $T_z$  are the Lagrangian integral time scales of the bubble motion.

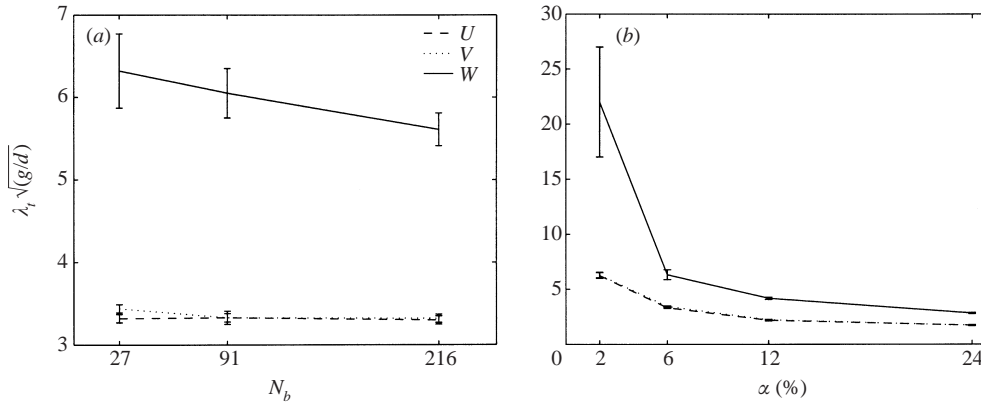


FIGURE 10. Taylor microscales  $\lambda_t$  of the autocorrelation functions of the bubble velocity fluctuations. Effect of (a) system size and (b) void fraction.

decrease as  $\alpha$  increases. The same quantitative trends for the correlation times are seen in the results of Ladd (1993), although Nicolai *et al.* (1995) report that the horizontal and vertical correlation times are both approximately equal to  $60t_s$  independently of the volume fraction in a range [5%, 40%],  $t_s$  being the Stokes time or time necessary for one isolated particle to fall one radius. These discrepancies highlight the need for further studies, in particular to determine more accurately the dispersion characteristics in the horizontal direction, since it appears that these are quite sensitive to system size effects.

The main statistical results for the transport properties of the bubbles are summarized in table 1.

### 3.3. Reynolds stresses and dissipation in the liquid phase

Although the flow field around a bubble remains laminar in the range of Reynolds numbers considered, averaging approaches used to model two-phase flows lead to the appearance of pseudo-turbulent terms characterizing the randomly fluctuating



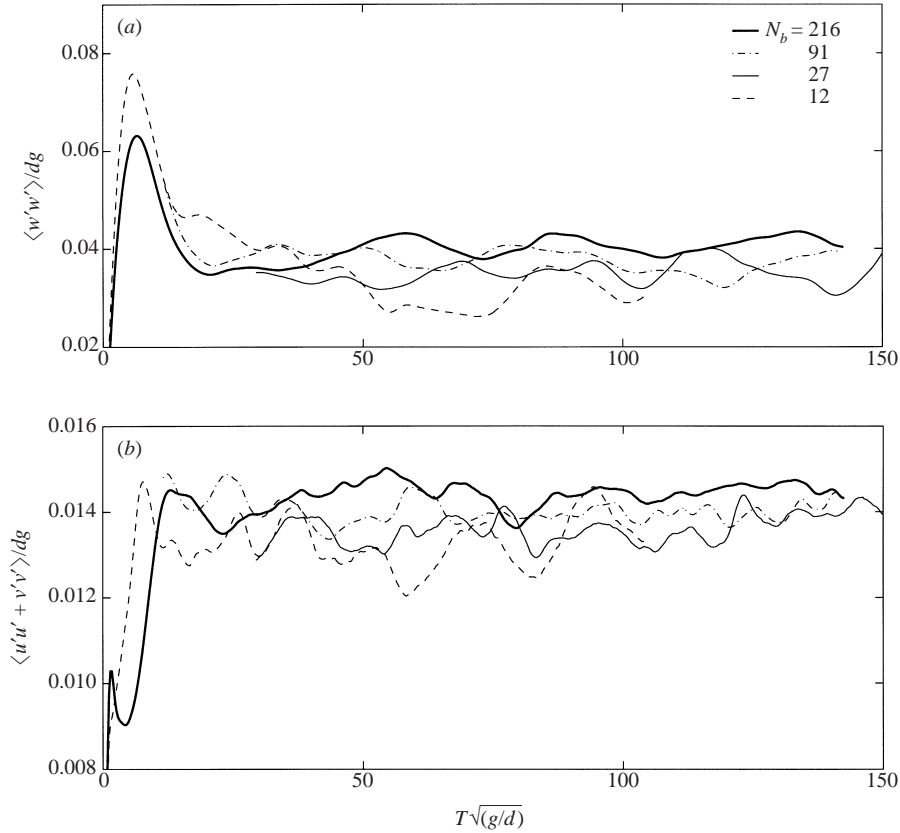


FIGURE 11. The (a) vertical and (b) horizontal Reynolds stresses vs. time for the different system sizes at  $\alpha = 6\%$ . The data for  $N_b = 27$  before  $t = 30$  and for  $N_b = 91$  before  $t = 12$  are missing.

velocity field produced by the bubbles. As in single-phase turbulence, two fundamental quantities are the Reynolds stress tensor and the rate of dissipation of turbulent kinetic energy in the continuous phase. The Reynolds stress per unit volume is defined as

$$\langle u'_i u'_j \rangle = \frac{1}{\Omega_f} \int_{\Omega_f} u'_i u'_j dV, \quad (3.11)$$

where  $\Omega_f$  is the volume occupied by the liquid in the periodic cell and  $u'_i$  is the fluctuating component of the liquid velocity in the  $i$  direction.

The flow field is initially quiescent. When the bubbles start rising, they retain their initial configuration for a short time and their rise velocity increases rapidly, after which the initial array breaks up, the bubbles redistribute themselves spatially, and the rise velocity decreases and settles down to a statistical steady state. A similar trend is seen in the evolution of the vertical Reynolds stress with time in figures 11(a) and 12(a). The vertical and horizontal Reynolds stresses in the liquid,  $\langle w'w' \rangle$  and  $\langle u'u' + v'v' \rangle$ , are shown versus time in figure 11 for different values of  $N_b$  and  $\alpha = 6\%$  and in figure 12 for different values of  $\alpha$  and  $N_b = 27$ . In contrast, the horizontal Reynolds stress, in figures 11(b) and 12(b), is lower in the initial transient than in the steady state because the motion of the bubbles is initially primarily vertical. Because of the symmetry of the problem and the absence of walls, it is expected that the off-diagonal components of the Reynolds stress tensor are zero and that  $\langle u'u' \rangle \approx \langle v'v' \rangle$ .

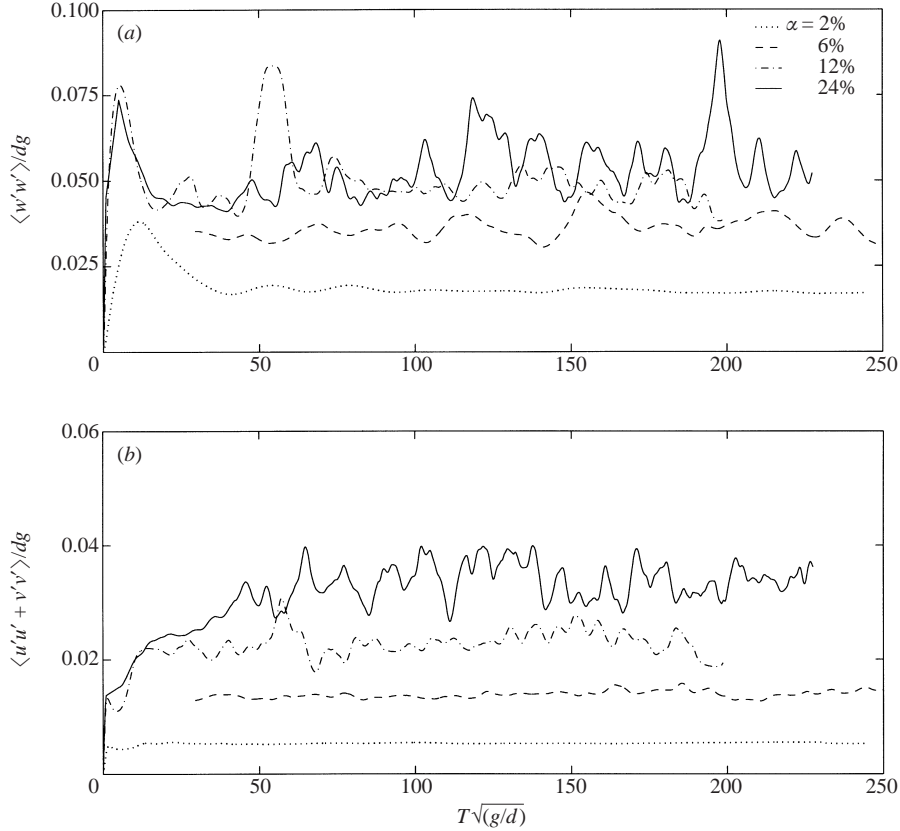


FIGURE 12. The (a) vertical and (b) horizontal Reynolds stresses vs. time for the different void fractions and  $N_b = 27$ . The data for  $\alpha = 6\%$  before  $t = 29$  are missing.

We verified that both conditions are satisfied to a good degree, especially for systems with large numbers of bubbles, the errors coming from the finite time interval used to average the values. Numerically, the off-diagonal components are always smaller than 5% of  $\langle w'w' \rangle$  and typically smaller than 1% of  $\langle w'w' \rangle$ . The results exhibit fluctuations in time that decrease when  $N_b$  increases and increase when  $\alpha$  increases, but a statistical steady state is reached in all cases.

The mean values over the  $[T_i, T_f]$  intervals are shown in figures 13 and 14, along with the turbulent kinetic energy,  $k = \langle u'u' + v'v' + w'w' \rangle / 2$ . Both components are dependent on the system size:  $\langle u'u' + v'v' \rangle^{1/2}$  increases by 1.9% between  $N_b = 27$  and  $N_b = 216$ , while  $\langle w'w' \rangle^{1/2}$  increases by an even larger amount, 6.0%. The increase in  $\langle w'w' \rangle^{1/2}$  is larger than the increase in the average rise velocity, which is 2%, but is of the same order of magnitude as the change in the bubble velocity fluctuations, whose vertical and horizontal components increase respectively by 4.8% and 21% (§ 3.1).

For the free arrays, both the vertical and horizontal Reynolds stresses increase with  $\alpha$ , but  $\langle u'u' + v'v' \rangle$  does so faster than  $\langle w'w' \rangle$ . As a consequence, the anisotropy diminishes, as can be seen in figure 14(d):  $\langle w'w' \rangle / \langle u'u' + v'v' \rangle$  goes from 3.3 to 1.6 between  $\alpha = 2\%$  and 24%. These values are comparable to the ratio of the squares of the vertical and horizontal bubble velocity fluctuations,  $W_b^2 / (U_b^2 + V_b^2)$ , which decreases from 5.7 to 1.9 between  $\alpha = 2\%$  and 24% (§ 3.1). The increased isotropy with void fraction shows that energy is being transferred from the rise direction to the

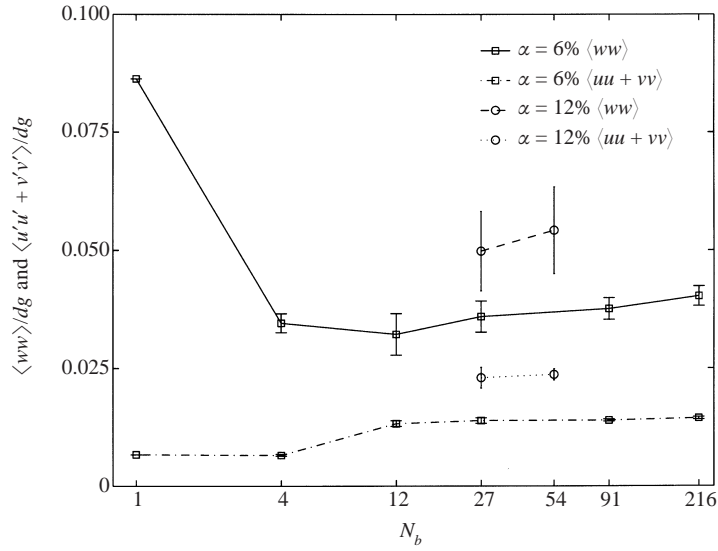


FIGURE 13. Effect of system size on the average Reynolds stresses for  $\alpha = 6\%$  and  $12\%$ .

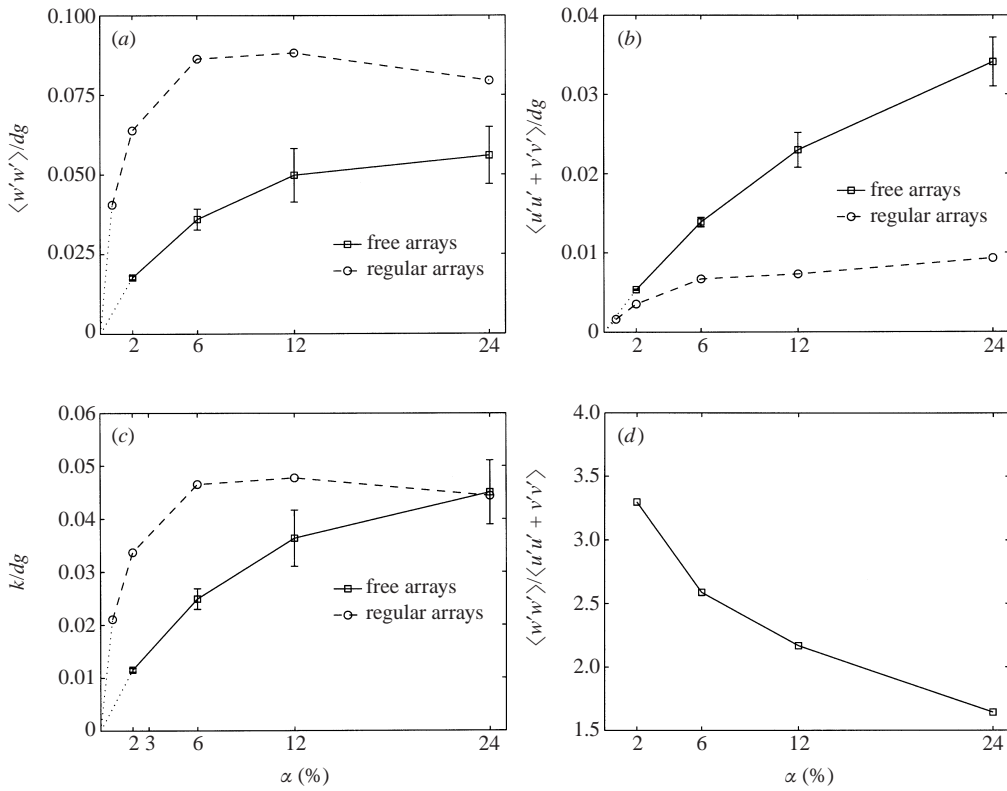


FIGURE 14. Effect of void fraction on the average Reynolds stresses and turbulent kinetic energy for the free arrays ( $N_b = 27$ ) and the regular arrays. (a) Vertical Reynolds stress; (b) horizontal Reynolds stress; (c) turbulent kinetic energy; (d) ratio of the vertical to horizontal Reynolds stresses in the free arrays.

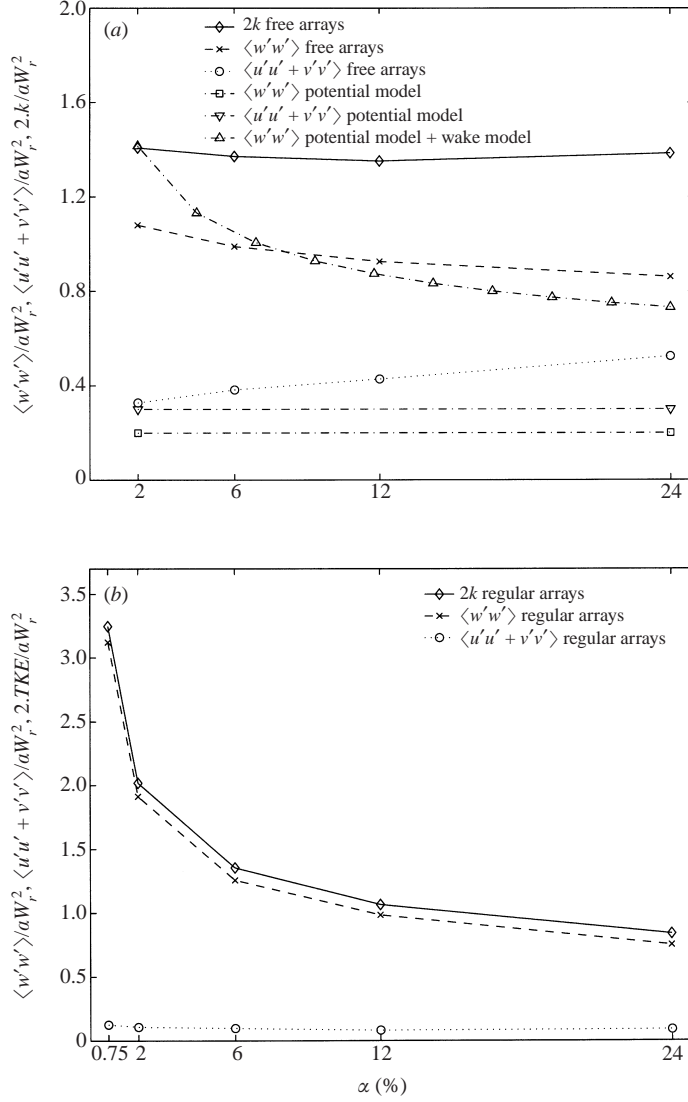


FIGURE 15. Scaling of the Reynolds stresses and the turbulent kinetic energy by  $\alpha W_r^2$  for (a) the free arrays with  $N_b = 27$  and (b) the regular arrays.

horizontal direction. For regular arrays,  $\langle w'w' \rangle$  increases until  $\alpha = 6\%$  and decreases for  $\alpha > 12\%$ , but is larger than the corresponding value in the free array;  $\langle u'u' + v'v' \rangle$  is much smaller in the regular arrays than in the free arrays because of the absence of lateral motion of the bubbles in the regular arrays.

The Reynolds stresses and the turbulent kinetic energy scaled by  $\alpha W_r^2$ , where  $W_r$  is the mean bubble rise velocity, are shown in figure 15. In the free arrays,  $\langle w'w' \rangle / \alpha W_r^2$  decreases slightly and  $\langle u'u' + v'v' \rangle / \alpha W_r^2$  increases slightly with  $\alpha$ , while  $k / \alpha W_r^2$  is nearly constant. The following scalings are obtained for the [2%, 24%] void fraction range:

$$\langle w'w' \rangle / \alpha W_r^2 = 0.97 \pm 0.11, \quad (3.12)$$

$$\langle u'u' + v'v' \rangle / \alpha W_r^2 = 0.43 \pm 0.09, \quad (3.13)$$

$$k / \alpha W_r^2 = 0.69 \pm 0.02. \quad (3.14)$$

Zenit *et al.* (2001) also found that the Reynolds stresses normalized by the squared bubble rise velocity increase linearly with  $\alpha$ , except in the vicinity of  $\alpha = 0$ . In addition, they observed similar levels of anisotropy between the vertical and horizontal components. However, their values are larger than ours by a factor of 2 to 3; for example, for  $\alpha = 12\%$ , they obtained  $\langle w'w' \rangle / \alpha W_r^2 \sim 2.9$  and  $\langle u'u' + v'v' \rangle / \alpha W_r^2 \sim 0.8$ . In addition to the difference in Reynolds numbers between their experiments and our simulations, their larger values might be due to the fact that their bubbles experienced significant deformations. For the regular arrays,  $\langle w'w' \rangle$  and  $k$  do not scale well with  $\alpha W_r^2$ , especially at low void fractions. For  $\alpha < 6\%$ ,  $k$  is much larger in the regular array than in the free array. For  $\alpha \geq 6\%$ , the value of  $\langle w'w' \rangle / \alpha W_r^2$  in the regular arrays is close to the value in the free array, suggesting that regular arrays can be used to provide rough estimates of the vertical Reynold stress in free arrays in the case of dense suspensions.

The inviscid solution for the flow around a sphere has been used by Drew & Lahey (1993) in order to estimate the Reynolds stress in the continuous phase. For spherical bubbles,

$$\langle u'_i u'_j \rangle = \begin{pmatrix} \frac{3}{20} & 0 & 0 \\ 0 & \frac{3}{20} & 0 \\ 0 & 0 & \frac{4}{20} \end{pmatrix} \alpha W_r^2. \quad (3.15)$$

The terms in equation (3.15) were identified by Lance & Bataille (1991) as the contribution to the Reynolds stress due to the kinematics of the bubbles, as opposed to the contribution due to the bubble wakes. They are shown in figure 15(a). The inviscid model underpredicts the simulation results by a factor of 5 for  $\langle w'w' \rangle$  and about 1.5 for  $\langle u'u' + v'v' \rangle$ . In addition, the inviscid model given by equation (3.15) predicts that the values of the three components of the Reynolds stress tensor are of the same order, whereas the simulation results show a strong anisotropy in favour of the vertical direction. These two observations suggest that the fluctuations produced by the wakes of the bubbles are responsible for a significant portion of the total fluctuating kinetic energy. Similar levels of anisotropy between the streamwise and the cross-stream Reynolds stresses are reported by Parthasarathy & Faeth (1990a) in a study of homogeneous dilute particle-laden flows caused by solid particles falling in a stagnant water bath. In contrast, in their measurement of the turbulence in air–water bubble flows for void fractions between 0 and 3%, Lance & Bataille (1991) found that the Reynolds stress tensor is nearly isotropic. They report that  $\langle w'w' \rangle / W_r^2$  is a linear function of  $\alpha$  and is in good agreement with the inviscid model for the contribution due to the bubble kinematics, which leads them to suggest that the wakes contribute only a small amount to the total fluctuating kinetic energy. Their experimental conditions are, however, very different from the conditions of our simulations. Lance & Bataille (1991) use large ellipsoidal bubbles which follow helicoidal trajectories and therefore induce large lateral motion in the fluid, whereas the parameters in our simulations are chosen such that bubbles rise approximately rectilinearly in dilute conditions.

Lance & Bataille (1991) give a rough measure of the contribution of the wakes to the Reynolds stress by noting that the dissipation rate due to the wake can be estimated by the work performed by the drag force experienced by the bubbles,

$$\epsilon_w \approx \frac{\alpha}{d} C_D W_r^3, \quad (3.16)$$

and by assuming that the velocity fluctuations  $u'_w$  associated with this dissipation

have a lengthscale  $l_w$ , so that

$$u_w'^2 \approx \left(\frac{\alpha}{d} C_{dlw}\right)^{2/3} W_r^2. \quad (3.17)$$

The contribution of this term is added to the contribution of the potential model; the total is shown in figure 15(a). The lengthscale representative of the dissipation in the wake is taken to be the width of the wake, for which a crude approximation is made by using Moore's estimate,  $l_w = aRe^{-1/4}$ , even though this expression has been established for higher Reynolds numbers. When the streamwise contributions of equations (3.15) and (3.17) are added, the result for  $\langle w'w' \rangle / \alpha W_r^2$  is of the same order of magnitude as the values found in the simulations, which confirms the importance of the contribution of the wake to the Reynolds stress.

We define the dissipation rate per unit volume in the gas and in the liquid phase,  $\epsilon_{ij}$ , and the dissipation rate per unit volume in the liquid phase only,  $\epsilon_{fij}$ , as

$$\epsilon_{ij} = \frac{1}{2\Omega} \int_{\Omega} \mu \left( \frac{\partial u_i}{\partial x_j} + \frac{\partial u_j}{\partial x_i} \right)^2 dV, \quad (3.18)$$

$$\epsilon_{fij} = \frac{1}{2\Omega_f} \int_{\Omega_f} \mu \left( \frac{\partial u_i}{\partial x_j} + \frac{\partial u_j}{\partial x_i} \right)^2 dV, \quad (3.19)$$

where  $\Omega$  and  $\Omega_f$  are the volumes of the entire domain and of the liquid phase, respectively. The total dissipation rate,  $\epsilon = \sum \epsilon_{ij}$ , can be related to the average bubble rise velocity by noting that the rate of work done by the bubbles on the fluid is balanced by the dissipation rate at steady state. Esmaceli & Tryggvason (1999) found

$$\epsilon = \frac{1}{\Omega} \int_{\Omega} (\rho_0 - \rho) \mathbf{u} \cdot \mathbf{g} dV = \alpha g W_r \rho_f (1 - \alpha + \alpha r)(1 - r), \quad (3.20)$$

where  $\rho_0$  is the volume-averaged density and  $r = \rho_b / \rho_f$  is the density ratio. The value of  $\epsilon$  scaled by the right-hand side of equation (3.20) is shown versus  $\alpha$  in figure 16, along with  $(1 - \alpha)\epsilon_f / \epsilon$ , where  $\epsilon_f = \sum \epsilon_{fij}$ . Equation (3.20) is satisfied to within 2–3% in both the free and regular arrays. It is interesting to note that  $(1 - \alpha)\epsilon_f / \epsilon$  is approximately constant and that the dissipation rate in the bubbly phase represents about 10% of the total dissipation rate  $\epsilon$ , irrespective of the void fraction, so that  $\alpha g W_r \rho_f (1 - \alpha + \alpha r)(1 - r)$  also provides a good scaling for the dissipation rate in the liquid only.

The different components of the dissipation rate tensor in the liquid phase,  $\epsilon_{fij}$ , are shown versus time for  $N_b = 216$  in figure 17 and versus  $\alpha$  for  $N_b = 27$  in figure 18. All values are scaled by  $\epsilon_f$ . For the free arrays, the vertical component,  $\epsilon_{fzz}$ , is twice as large as the horizontal components,  $\epsilon_{fxx}$  and  $\epsilon_{fyy}$ . In absolute value, all components of  $\epsilon_{fij}$  increase monotonically with  $\alpha$ . Finally, we note that, like the rise velocity, the results are approximately independent of system size for  $N_b \geq 12$ .

The main properties of the liquid-phase turbulence are summarized in table 2 for the free arrays. The Kolmogorov lengthscale  $l_K$  and the Taylor microscale  $\lambda$ , defined in table 2, decrease slightly as the void fraction increases. Because of the low Reynolds number,  $\lambda$  is only two to three times larger than  $l_K$ , whereas it is about one hundred times larger in the experiments of Lance & Bataille (1991), where the Reynolds numbers are much larger. The Kolmogorov lengthscale is always much smaller than the bubble diameter. In numerical simulations of particulate flows, the Kolmogorov

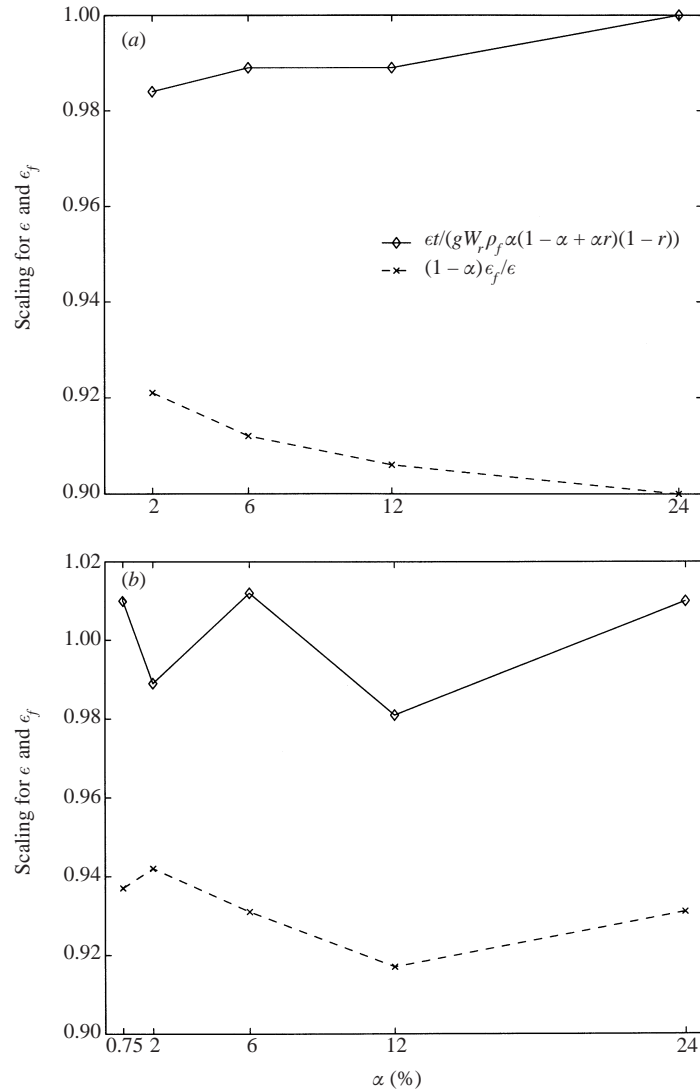


FIGURE 16. Scaling of the total dissipation rate by the average velocity of the bubbles relative to the liquid and ratio of the dissipation rate in the liquid to the total dissipation rate for the (a) free arrays with  $N_b = 27$  and (b) regular arrays.

lengthscale is often assumed to be larger than the particles, so that the particles can be modelled as points (e.g. Squires & Eaton 1990; Elghobashi & Truesdell 1992; Wang & Maxey 1993). Such an assumption is impossible for typical bubbly flows. For example, in the experiments of Lance & Bataille (1991),  $d$  is about 5 mm while  $l_K$  is about 0.01 mm. Numerical simulations of bubbly flows must therefore account for all scales of motion.

#### 3.4. Kinetic energy spectrum

As pointed out by Sundaram & Collins (1999), two-equation models of turbulence assume that the energy spectrum can be described by two quantities such as the kinetic energy and dissipation rate of kinetic energy. In multiphase flows, it is not

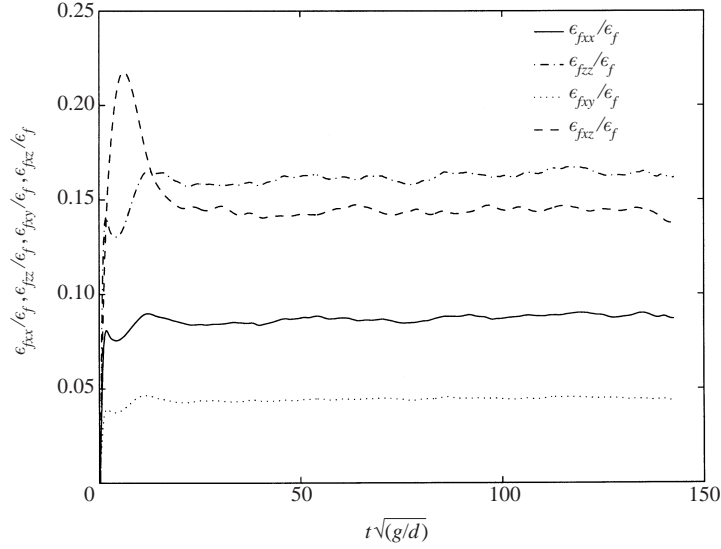


FIGURE 17. The components of the dissipation rate tensor in the liquid scaled by the total dissipation rate in the liquid as a function of time for  $N_b = 216$ .

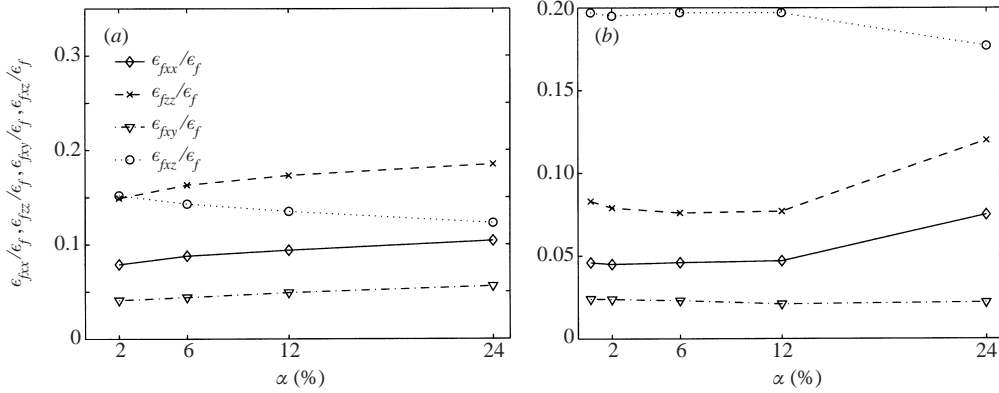


FIGURE 18. The components of the dissipation rate tensor in the liquid divided by the total dissipation rate in the liquid for the (a) free arrays with  $N_b = 27$  and (b) regular arrays.

clear if such a universal spectrum exists. In this section, we examine the isotropic kinetic spectrum to determine whether it settles down to a steady-state shape, how it depends on the system size, and how it depends on the void fraction.

To examine the structure of the velocity field, we determine the isotropic kinetic energy spectrum,  $E(k)$ . The spectrum is computed from the velocity field  $\mathbf{u}$  and density field  $\rho$  in the entire computational domain and is normalized so that  $\sum_k E(k)\Delta k = \frac{1}{2} \int_{\Omega} \rho \|\mathbf{u}\|^2 dV$ . First, the discrete Fourier transforms of the velocities multiplied by the square root of the density are calculated. Then the energy content is summed in spherical shells of width  $\Delta k$  centred at  $k = (k_x^2 + k_y^2 + k_z^2)^{1/2}$ . An isotropic spectrum is commonly used even in situations which are clearly anisotropic such as the rise of bubbles.

The kinetic energy spectrum is shown at different times for  $N_b = 27$ ,  $\alpha = 6\%$  in figure 19. At  $t = 8.6$ , the bubbles are in their initial transient phase. Since the initial



$\alpha$ (%)	$N_b$	$Re_r$	$\frac{\langle w'w' \rangle}{gd}$ ( $10^{-2}$ )	$\frac{\langle u'u' + v'v' \rangle}{gd}$ ( $10^{-2}$ )	$\frac{\epsilon_f}{\rho_f \sqrt{g^3 d}}$ ( $10^{-2}$ )	$\frac{l_K}{d}$	$\frac{u_K}{W_b}$	$\frac{\lambda}{d}$	$Re_\lambda$
2	27	27.14	1.77	0.54	1.61	0.219	0.168	0.489	1.29
6	4	21.48	3.46	0.66	3.54	0.180	0.259	0.441	1.55
6	12	23.26	3.22	1.33	4.00	0.174	0.249	0.436	1.61
6	27	23.35	3.59	1.39	4.14	0.173	0.248	0.448	1.76
6	91	23.61	3.76	1.40	4.13	0.173	0.245	0.456	1.80
6	216	23.82	4.03	1.44	4.17	0.173	0.243	0.468	1.90
12	27	20.09	4.98	2.30	7.07	0.151	0.329	0.414	1.94
12	54	20.38	5.42	2.37	7.06	0.151	0.324	0.429	2.07
24	27	15.62	5.60	3.41	11.1	0.135	0.474	0.368	1.92

TABLE 2. Properties of the turbulence in the liquid: vertical and horizontal Reynolds stresses  $\langle w'w' \rangle$  and  $\langle u'u' + v'v' \rangle$ , dissipation rate per unit volume of liquid,  $\epsilon_f$ , Kolmogorov length and velocity scales  $l_K$  and  $u_K$ , Taylor microscale  $\lambda$ , microscale Reynolds number  $Re_\lambda$ . The Kolmogorov scales are determined according to  $l_K = (v_f^3 \rho_f / \epsilon_f)^{1/4}$  and  $u_K = (\epsilon_f \nu_f / \rho_f)^{1/4}$ . Note that  $\epsilon_f / \rho_f$  represents the dissipation rate per unit mass.  $\lambda$  is evaluated roughly by using the single-phase formula for homogeneous isotropic turbulence,  $\epsilon_f = 15 \nu_f u'^2 / \lambda^2$ , where  $u'$  is the r.m.s velocity determined from the turbulent kinetic energy in the liquid,  $u' = (2k_f/3)^{1/2}$ , and  $k_f = \langle u'u' + v'v' + w'w' \rangle / 2$  (Tennekes & Lumley 1972).  $Re_\lambda$  is defined as  $Re_\lambda = \rho_f u' \lambda / \mu_f$ . The mean rise Reynolds number of the bubbles,  $Re_r$ , based on the slip velocity of the bubbles relative to the liquid, is added for reference.

flow field is quiescent and no external forcing is applied, the long waves contain little energy immediately after the bubbles are released. The peak at  $kd = 3.04$  corresponds to the average horizontal or vertical distance between neighbouring bubbles in the initial perturbed array, which is the mode being excited. As pointed out by Esmaeeli & Tryggvason (1996), the bubbles can be viewed as a stirring force acting on the fluid. As time increases, energy is fed by the bubbles into the long-wave components of the spectrum. However, unlike the two-dimensional results of Esmaeeli & Tryggvason (1996), there exists a statistical steady state, where the production of energy by the bubbles balances the dissipation of energy in the liquid. In particular, no large-scale flow structure is observed. Since the number of bubbles is small and effects of system size are visible in the results for the bubble velocity fluctuations up to  $N_b \leq 216$ , as seen in § 3.1, it is possible that large-scale flow structures would appear in larger simulations, but we believe that it is unlikely for two reasons. First, no trend toward the formation of such structures can be seen in our results. Figure 20 shows the kinetic energy spectrum for  $N_b = 27, 91$  and  $216$  at the same time. The spectra are almost identical. The small differences at low wavenumbers can be attributed to the fluctuations in time of the total kinetic energy. Second, the mechanisms responsible for the interaction of two bubbles, which were described in Part 1, § 3.3, tend to homogenize the spatial distribution of the bubbles. When two bubbles are aligned side by side, they tend to repel each other. When they are aligned in tandem, the trailing bubble is attracted into the wake of the leading bubble, but this configuration is unstable and the two bubbles eventually tumble about each other. Strikingly different results are obtained for ellipsoidal bubbles, which form vertical streams due to a change in the lift force when the bubbles are deformable (Bunner & Tryggvason 2002b).

The effect of void fraction on the kinetic energy spectrum and on the dissipation rate spectrum is illustrated in figure 21 for  $N_b = 27$ . The dissipation rate spectrum

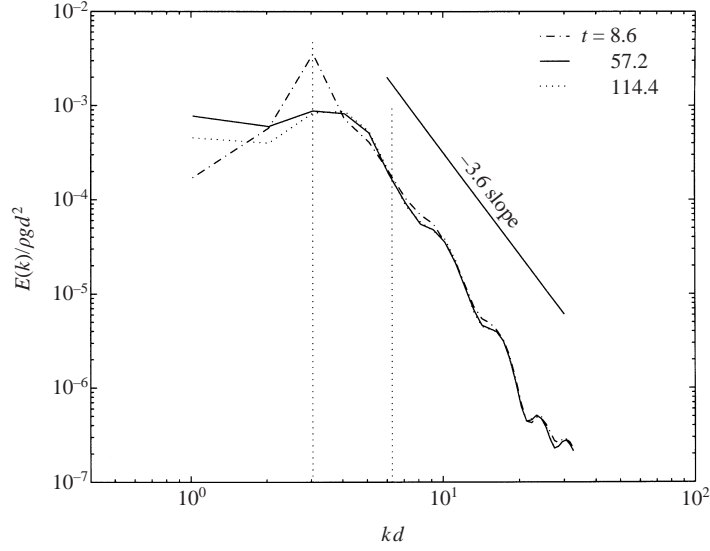


FIGURE 19. Kinetic energy spectrum for  $N_b = 27$ ,  $\alpha = 6\%$  at three different times. The dotted vertical lines indicate the wavenumbers corresponding to the mean spacing between the bubbles' centroids,  $kd = 3.04$ , and the bubble diameter,  $kd = 6.28$ . The Kolmogorov length scale, not shown, corresponds to  $kd = 36.3$ . Since this simulation was performed on a  $128^3$  grid, the curves should have 64 points from  $kd = 1.02$  to  $kd = 65.08$ . However, due to memory restrictions in the postprocessing, only the first 32 points, from  $kd = 1.02$  to  $kd = 32.38$ , are determined.

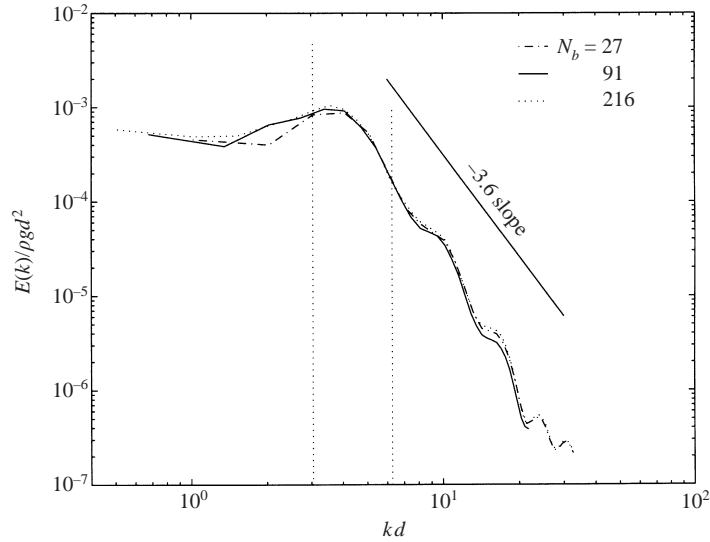


FIGURE 20. Effect of system size on the kinetic energy spectrum at  $\alpha = 6\%$ ,  $t = 114.4$ . The dotted vertical lines indicate the wavenumbers corresponding to the mean spacing between the bubbles' centroids,  $kd = 3.04$ , and the bubble diameter,  $kd = 6.28$ . The Kolmogorov length scale, not shown, corresponds to  $kd = 36.3$ .

is defined as  $D(k) = 2\nu k^2 E(k)$  and satisfies  $\sum_k D(k) \Delta k = \epsilon$ . When the flow reaches steady state, the maximum in the kinetic energy spectra is at the wavenumber corresponding to the mean spacing distance between the bubbles, indicating that the larger contribution to the velocity fluctuations comes from the correlated motion

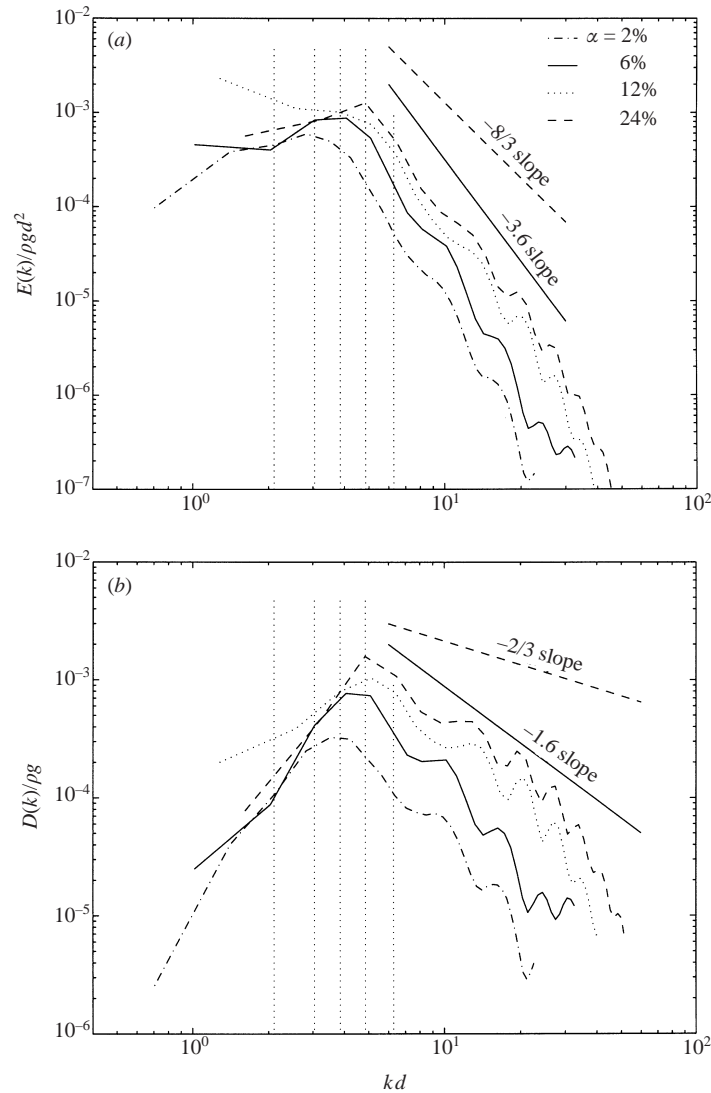


FIGURE 21. Effect of void fraction on the (a) kinetic energy spectrum and (b) dissipation rate spectrum for  $N_b = 27$ . The vertical lines correspond, from left to right, to the mean spacings between the bubbles' centroids, which are respectively  $kd = 2.10, 3.04, 3.85$  and  $4.86$  for  $\alpha = 2\%$ ,  $6\%$ ,  $12\%$  and  $24\%$ , and to the bubble diameter,  $kd = 6.28$ .

of many bubbles rather than from the summation of the disturbances created by individual bubbles, as was pointed out by Zenit *et al.* (2001). As the void fraction increases, the wavenumber at the maximum of the spectrum increases too. In addition, the spectrum is shifted upwards because of the increase in kinetic energy of the liquid. For all cases considered, however, the kinetic energy spectrum decays with the same slope for  $kd > 6.28$ . As remarked in Zenit *et al.* (2001), this is due to the fact that the fluctuations at these wavenumbers are produced by structures smaller than the size of the bubbles. This slope is approximately  $-3.6$  and is added to figures 19, 20 and 21(a). In figure 21(a), the  $-8/3$  slope found in the experiments of Lance & Bataille (1991) is also shown. The fact that the slope is higher in our results than in

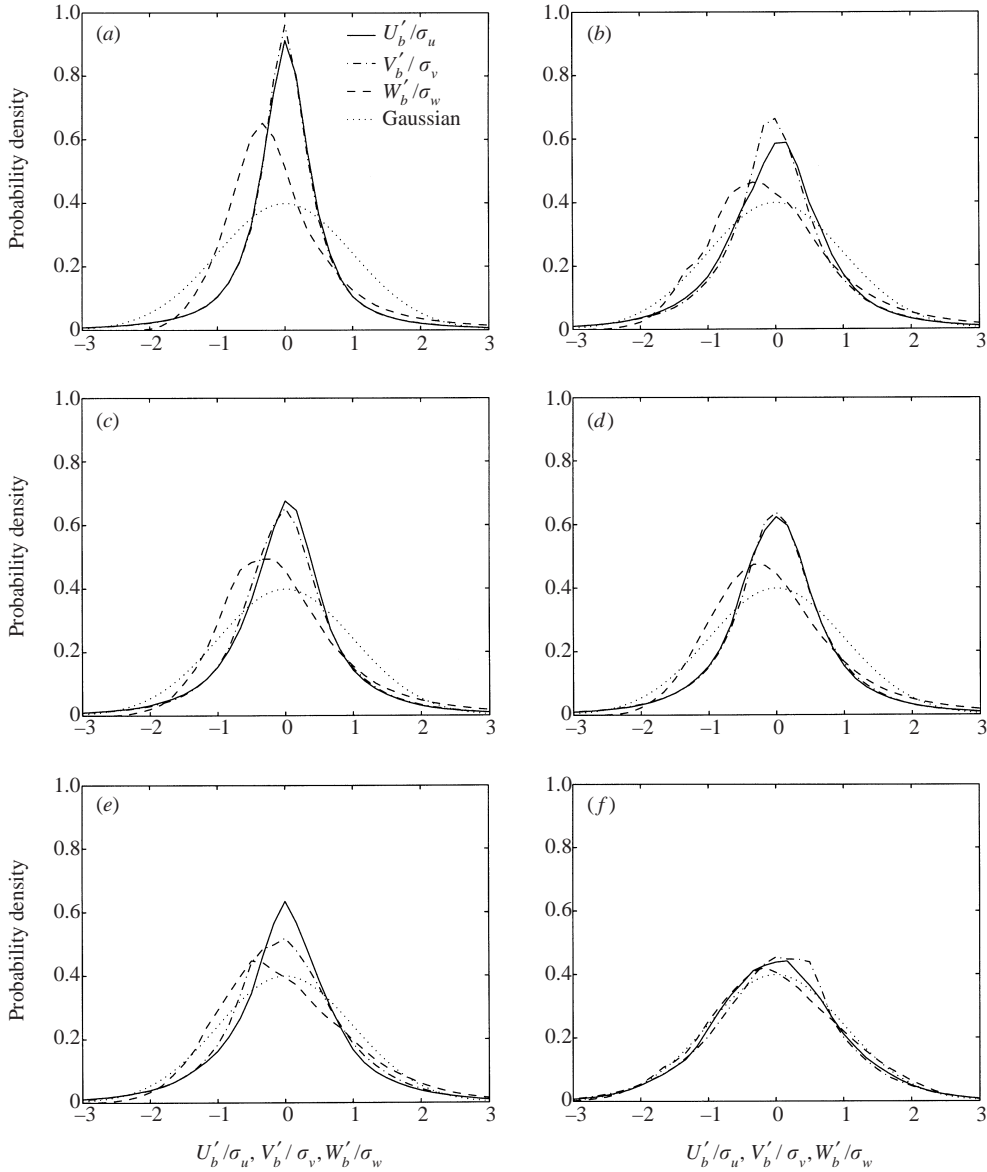


FIGURE 22. Probability density function of the liquid velocity fluctuations. (a)  $\alpha = 2\%$ ; (b)  $\alpha = 6\%$ ,  $N_b = 27$ ; (c)  $\alpha = 6\%$ ,  $N_b = 91$ ; (d)  $\alpha = 6\%$ ,  $N_b = 216$ ; (e)  $\alpha = 12\%$ , (f)  $\alpha = 24\%$ .

the experiments of Lance & Bataille (1991) can be attributed to the very different conditions of our simulations, which are for laminar, low-Reynolds-number bubbly flows, and their experiments, which were for turbulent, high-Reynolds-number bubbly flows. Also, there is a considerable amount of uncertainty in the evaluation of the slope from our results since the data span only a limited range of wavenumbers. In particular, the fluctuations seen at high wavenumbers in the spectra are due to the rapid changes in density and velocity across the interface between the outer fluid and the bubbles. Both slopes are however much larger than the classical  $-5/3$  power law in the inertial region of single-phase turbulent flows. Lance & Bataille (1991)

proposed an explanation for the higher slopes seen in bubbly flows. Using arguments of dimensional analysis and scaling for the spectral energy balance, they showed that the eddies produced in the wakes of the bubbles are dissipated by viscosity before any spectral transfer of energy can take place. As a result, the spectral energy balance reduces to a simple expression, which leads to  $E \approx k^{-3}$ , which is close to their findings as well as ours.

Finally, the probability density of the liquid velocity fluctuations is plotted in figure 22. The values are scaled by their standard deviation. The Gaussian curve with mean zero and standard deviation one is superposed on the plots. The p.d.f.s of the cross-stream velocities are symmetric with respect to a vertical line going through the zero point, whereas the vertical velocity curves are tilted towards the region of negative velocity. The results exhibit considerable differences from the Gaussian profile, especially at low void fractions. A narrow peak is observed at  $\alpha = 2\%$ , which broadens as  $\alpha$  increases. This peak is more pronounced for the horizontal than for the vertical velocity fluctuations. These two observations are consistent with the experimental findings of Zenit *et al.* (2001). The reason for the non-Gaussian p.d.f.s is presumably due to the way the bubbles interact. At low void fractions, the bubbles interact by the ‘drafting, kissing, and tumbling’ mechanism, where the bubbles accelerate in the wake of the bubble in the front. This should result in a relatively narrow range of velocity fluctuations in the liquid. As the void fraction increases, the presence of other bubbles results in more complex and more random interactions.

#### 4. Conclusion

This paper is the second part of an investigation of finite Reynolds number bubbly flows. The Reynolds number lies between 12 and 30, depending on the void fraction, which varies between 2% and 24%. The effects of viscosity, inertia and surface tension are all accounted for. Part 1 considered the rise velocity and the microstructure of the bubbles. Part 2 analyses the properties of the fluctuation velocity of the bubbles and the liquid-phase turbulence. The major observations are as follows:

(i) The fluctuation velocities of the bubbles and the Reynolds stress in the liquid increase when the number of bubbles in the periodic cell,  $N_b$ , increases. We were not able to determine the limit values of both quantities, even with  $N_b = 216$ .

(ii) The vertical fluctuation velocities of both the bubbles and the liquid are larger than the horizontal fluctuation velocities. The anisotropy decreases as the void fraction increases. The variance of the bubble velocities, i.e. the square of the total fluctuation velocities of the bubbles, and the turbulent kinetic energy scale with  $\alpha W_r^2$ , where  $W_r$  is the relative velocity of the bubbles relative to the liquid.

(iii) The self-dispersion of the bubbles can be roughly characterized as Gaussian with a strongly anisotropic dispersion coefficient tensor. The vertical dispersion coefficient is maximum at  $\alpha = 12\%$ , where it is equal to  $1.2\alpha W_r$ . Even though the results are affected by the small size of the systems, it appears that the dispersion coefficients in the self-diffusion of bubbles are much smaller than their counterparts in the self-diffusion of solid particles.

(iv) The kinetic energy spectrum follows a  $-3.6$  power law at large wavenumbers. This is of the same order as the value of  $-8/3$  seen in the experiments of Lance & Bataille (1991).

This study shows the feasibility of performing large-scale direct numerical simulations of dispersed multiphase flows to complement experiments and assist in modelling

by providing a detailed picture of the flow. A study of a monodisperse suspension of bubbles is a first step in developing a thorough understanding of bubbly flows. Future studies should consider the effects of polydispersion, surfactants, coalescence, breakup and higher Reynolds numbers.

One important question is left unanswered by this study: What happens when the number of bubbles increases beyond  $N_b = 216$ ? One possibility is the appearance of large-scale flow structures such as the recirculation loops commonly seen in bubble columns. We do not believe that this will happen, at least for spherical bubbles and  $\alpha \leq 12\%$  because the mechanisms of interaction between the bubbles tend to homogenize their spatial distribution. Nevertheless, larger simulations including more bubbles are necessary to verify this hypothesis and to obtain results for the fluctuation velocities and the dispersion coefficients, which are independent of  $N_b$ . For highly deformable bubbles, the interaction mechanisms are different and do lead to the formation of large-scale flow structures (Bunner & Tryggvason 2002*b*).

The authors gratefully acknowledge the support of the National Science Foundation under grant CTS-9503208 and of the University of Michigan through a Rackham Predoctoral Fellowship. This research was supported in part by NSF cooperative agreement ACI-9619020 through computing resources provided by the National Partnership for Advanced Computational Infrastructure at the University of Michigan Center for Parallel Computing. In addition, this research, in part conducted at the Maui High Performance Computing Center, was sponsored in part by the Air Force Research Laboratory, Air Force Materiel Command, USAF, under cooperative agreement number F29601-93-2-0001. The views and conclusions contained in this document are those of the authors and should not be interpreted as necessarily representing the official policies or endorsements, either expressed or implied, of the Air Force Research Laboratory, the US Government, the University of New Mexico, or the Maui High Performance Computing Center.

#### REFERENCES

- ACRIVOS, A., BATCHELOR, G. K., HINCH, E. J., KOCH, D. L. & MAURI, R. 1992 Longitudinal shear-induced diffusion of spheres in a dilute suspension. *J. Fluid Mech.* **240**, 651–657.
- BATCHELOR, G. K. & TOWNSEND, A. A. 1956 Turbulent diffusion. *Surveys in Mechanics*. Cambridge University Press.
- BRENNER, M. P. 1999 Screening mechanisms in sedimentation. *Phys. Fluids* **11**, 754–771.
- BUNNER, B. & TRYGGVASON, G. 2002*a* Dynamics of homogeneous bubbly flows. Part 1. Rise velocity and microstructure of the bubbles. *J. Fluid Mech.* **466**, 17–52.
- BUNNER, B. & TRYGGVASON, G. 2002*b* Effect of bubble deformation on the stability and properties of bubble flows. Submitted to *J. Fluid Mech.*
- CAFLISCH, R. E. & LUKE, J. H. C. 1985 Variance in the sedimentation speed of a suspension. *Phys. Fluids* **28**, 759–760.
- CARTELLIER, A. & RIVIÈRE, N. 2001 Bubble-induced agitation and microstructure in uniform bubbly flows at small to moderate particle Reynolds numbers. *Phys. Fluids* **13**, 2165–2181.
- CROWE, C. T., TROUTT, T. R. & CHUNG, J. N. 1996 Numerical models for two-phase turbulent flows. *Annu. Rev. Fluid Mech.* **26**, 11–43.
- DAVIS, R. H. & HASSEN, M. A. 1988 Spreading of the interface at the top of a slightly polydisperse sedimenting suspension. *J. Fluid Mech.* **196**, 107–134.
- DAVIS, R. H. 1996 Hydrodynamic diffusion of suspended particles: a symposium. *J. Fluid Mech.* **310**, 325–335.
- DREW, D. A. & LAHEY, R. T. JR. 1993 Analytical modeling of multiphase flow. In *Particulate Two-phase flow* (ed. M. C. Roco), pp. 509–566. Butterworth.

- ECKSTEIN, E. C., BAILEY, D. G. & SHAPIRO, A. H. 1977 Self-diffusion in shear flow of a suspension. *J. Fluid Mech.* **79**, 191–208.
- ELGHOBASHI, S. E. & TRUESDELL, G. C. 1992 Direct simulation of particle dispersion in decaying isotropic turbulence. *J. Fluid Mech.* **242**, 655–700.
- ESMAEELI, A. & TRYGGVASON, G. 1996 An inverse energy cascade in two-dimensional, low Reynolds-number bubbly flows. *J. Fluid Mech.* **314**, 315–330.
- ESMAEELI, A. & TRYGGVASON, G. 1999 Direct numerical simulations of bubbly flows. Part 2. Moderate Reynolds number arrays. *J. Fluid Mech.* **385**, 325–358.
- HAM, J. M. & HOMSY, G. M. 1988 Hindered settling and hydrodynamic dispersion in quiescent sedimenting suspensions. *Intl J. Multiphase Flow* **14**, 533–546.
- KOCH, D. L. & SHAQFEH, E. S. G. 1991 Screening in sedimenting suspensions. *J. Fluid Mech.* **224**, 275–303.
- KOCH, D. L. 1993 Hydrodynamic diffusion in dilute sedimenting suspensions at moderate Reynolds numbers. *Phys. Fluids A* **5**, 1141–1155.
- LADD, A. J. C. 1993 Dynamical simulations of sedimenting spheres. *Phys. Fluids A* **5**, 299–310.
- LADD, A. J. C. 1997 Sedimentation of homogeneous suspensions of non-Brownian spheres. *Phys. Fluids* **9**, 491–499.
- LANCE, M. & BATAILLE, J. 1991 Turbulence in the liquid phase of a uniform bubbly air-water flow. *J. Fluid Mech.* **222**, 95–118.
- LEIGHTON, D. & ACRIVOS, A. 1987 Measurement of shear-induced self-diffusion on concentrated suspensions of spheres. *J. Fluid Mech.* **177**, 109–131.
- NICOLAI, H. & GUAZZELLI, E. 1995 Effect of the vessel size on the hydrodynamic diffusion of sedimenting spheres. *Phys. Fluids* **7**, 3–5.
- NICOLAI, H., HERZHAFT, B., HINCH, E. J., OGER, L. & GUAZZELLI, E. 1995 Particle velocity fluctuations and hydrodynamic self-diffusion of sedimenting non-Brownian spheres. *Phys. Fluids* **7**, 12–23.
- NITSCHKE, J. M. & BATCHELOR, G. K. 1997 Break-up of a falling drop containing dispersed particles. *J. Fluid Mech.* **340**, 161–175.
- PARTHASARATHY, R. N. & FAETH, G. M. 1990a Turbulence modulation in homogeneous dilute particle-laden flows. *J. Fluid Mech.* **220**, 485–514.
- PARTHASARATHY, R. N. & FAETH, G. M. 1990b Turbulent dispersion of particles in self-generated homogeneous turbulence. *J. Fluid Mech.* **220**, 515–537.
- POORTE, R. E. G. 1998 On the motion of bubbles in active grid generate turbulent flows. PhD Thesis, The University of Twente.
- RAHMAN, A. 1964 Correlations in the motion of atoms in liquid argon. *Phys. Rev.* **136** (2A), 405–411.
- SANGANI, A. S., ZHANG, D. Z. & PROSPERETTI, A. 1991 The added mass, Basset, and viscous drag coefficients in nondilute bubbly liquids undergoing small-amplitude oscillatory motion. *Phys. Fluids A* **3**, 2955–2970.
- SANGANI, A. S. & DIDWANIA, A. K. 1993 Dynamic simulations of flows of bubbly liquids at large Reynolds numbers. *J. Fluid Mech.* **250**, 307–337.
- SEGRÉ, P. N., HERBOLZHEIMER, E. & CHAIKIN, P. M. Long-range correlations in sedimentation. *Phys. Rev. Lett.* **79**, 2574–2577.
- SERIZAWA, A., KATAOKA, I. & MICHYOSHI, I. 1975 Turbulence structure of air-water bubbly flow. III Transport properties. *Intl J. Multiphase Flow* **2**, 247–259.
- SMERKA, P. 1993 On the motion of bubbles in a periodic box. *J. Fluid Mech.* **254**, 79–112.
- SNYDER, W. H. & LUMLEY, J. L. 1971 Some measurements of particle velocity autocorrelation functions in a turbulent flow. *J. Fluid Mech.* **48**, 41–71.
- SOKOLICHIN, A., EIGENBERGER, G., LAPIN, A. & LÜBBERT, A. 1997 Dynamic numerical simulation of gas-liquid two-phase flows: Euler-Euler versus Euler-Lagrange. *Chem. Engng Sci.* **52**, 611–626.
- SOMMERFELD, M., KOHNEN, G. & RÜGER, M. 1993 Some open questions and inconsistencies of Lagrangian particle dispersion models. *Proc. Ninth Symp. on Turbulent Shear Flows, Kyoto, Japan*.
- SPELT, P. D. M. & BIESHEUVEL, A. 1997 On the motion of gas bubbles in homogeneous isotropic turbulence. *J. Fluid Mech.* **336**, 221–244.
- SPELT, P. D. M. & BIESHEUVEL, A. 1998 Dispersion of gas bubbles in large-scale homogeneous isotropic turbulence. *Appl. Sci. Res.* **58**, 463–482.

- SPELT, P. D. M. & SANGANI, A. S. 1998 Properties and averaged equations for flows of bubbly liquids. *Appl. Sci. Res.* **58**, 337–386.
- SQUIRES, K. D. & EATON, J. K. 1990 Particle response and turbulence modification in isotropic turbulence. *Phys. Fluids A* **2**, 1191–1203.
- TAYLOR, G. I. 1921 Diffusion by continuous movements. *Proc. Lond. Math. Soc.* **20**, 196–212.
- SUNDARAM, S. & COLLINS, L. R. 1999 A numerical study of the modulation of isotropic turbulence by suspended particles. *J. Fluid Mech.* **379**, 105–143.
- TENNEKES, H. & LUMLEY, J. L. 1972 *A First Course in Turbulence*. The MIT Press.
- TRYGGVASON, G., BUNNER, B., ESMAEELI, A., JURIC, D., AL-RAWAHI, N., TAUBER, W., HAN, J., NAS, S. & JAN, Y.-J. 2001 A front tracking method for the computations of multiphase flow. *J. Comput. Phys.* **169**, 708–759.
- UNVERDI, S. O. & TRYGGVASON, G. 1992 A front-tracking method for viscous, incompressible, multi-fluid flows. *J. Comput Phys.* **100**, 25–37.
- WANG, L.-P. & MAXEY, M. R. 1993 Settling velocity and concentration distribution of heavy particles in homogeneous isotropic turbulence. *J. Fluid Mech.* **256**, 27–68.
- VAN WIJNGAARDEN, L. 1998 On pseudo-turbulence *Theoret. Comput. Fluid Dyn.* **10**, 449–458.
- YURKOVETSKY, Y. & BRADY, J. 1996 Statistical mechanics of bubbly liquids. *Phys. Fluids* **8**, 881–895.
- ZENIT, R., KOCH, D. L. & SANGANI, A. S. 2001 Measurements of the average properties of a suspension of bubbles rising in a vertical channel. *J. Fluid Mech.* **429**, 307–341.